Chemical Science

ROYAL SOCIETY OF CHEMISTRY

EDGE ARTICLE

View Article Online
View Journal | View Issue

Cite this: *Chem. Sci.*, 2023, **14**, 2386

All publication charges for this article have been paid for by the Royal Society of Chemistry

Next-generation membrane-active glycopeptide antibiotics that also inhibit bacterial cell division†

Paramita Sarkar,[a] Kathakali De,[a] Malvika Modi,[b] Geetika Dhanda,[a] Richa Priyadarshini,[b] Julia E. Bandow[c] and Jayanta Haldar *[a]

Received 9th October 2022
Accepted 2nd January 2023

DOI: 10.1039/d2sc05600c

rsc.li/chemical-science

Resistance to vancomycin, a life-saving drug against Gram-positive bacterial infections necessitates developing alternative therapeutics. Herein, we report vancomycin derivatives that assimilate mechanisms beyond D-Ala–D-Ala binding. The role of hydrophobicity towards the structure and function of the membrane-active vancomycin showed that alkyl-cationic substitutions favored broad-spectrum activity. The lead molecule, VanQAmC$_{10}$ delocalized the cell division protein MinD in *Bacillus subtilis*, implying an impact on bacterial cell division. Further examination of wild-type, GFP-FtsZ, or GFP-FtsI producing- and Δ*amiAC* mutants of *Escherichia coli* revealed filamentous phenotypes and delocalization of the FtsI protein. The findings indicate that VanQAmC$_{10}$ also inhibits bacterial cell division, a property previously unknown for glycopeptide antibiotics. The conjunction of multiple mechanisms contributes to its superior efficacy against metabolically active and inactive bacteria, wherein vancomycin is ineffective. Additionally, VanQAmC$_{10}$ exhibits high efficacy against methicillin-resistant *Staphylococcus aureus* (MRSA) and *Acinetobacter baumannii* in mouse models of infection.

Introduction

Vancomycin is a critically important antibiotic, that was the drug of last resort against infections caused by multidrug-resistant Gram-positive bacteria.[1] It belongs to the glycopeptide class of antibiotics that consists of naturally occurring and semi-synthetic products that inhibit bacterial cell wall biosynthesis by binding to the D-Ala–D-Ala terminus of the cell wall precursor pentapeptide.[1,2] However, widespread resistance to vancomycin that involves modification of the target peptide to D-Ala–D-Lac/D-Ser, concomitant with a reduction in binding affinity, and/or thickening of the cell wall has been reported.[3] To incorporate additional mechanisms, second-generation glycopeptide antibiotics, telavancin, dalbavancin, and oritavancin, were equipped with lipophilic substitutions that abetted destabilization of the bacterial membranes.[4] Despite reports of various modified glycopeptides that overcome inherited resistance,[3,5–10] there are only a few reports of derivatives that are effective against Gram-negative bacteria and dormant bacteria.[11–15] The presence of an outer membrane in Gram-negative bacteria (GNB) precludes entry of numerous antibiotics including glycopeptides.[16] Although the conjugation of membrane-interacting moieties onto glycopeptide antibiotics has shown activity against vancomycin-resistant Gram-positive bacteria, they do not necessarily result in activity against Gram-negative bacteria.[17]

We had developed C-terminally modified cationic lipophilic vancomycin derivatives that were effective against both vancomycin-resistant Gram-positive and the intrinsically resistant Gram-negative bacteria.[18–20] Their broad-spectrum antibacterial activity was attributed to the incorporation of membrane–perturbation properties through the conjugation of lipophilic cationic moieties. In this report, we first examine the structure–activity relationship of alkyl and aryl moieties as hydrophobic substituents and identify the most selective compound. The effect of various hydrophobic group substitutions on membrane perturbing ability, the antibacterial activity of exponential growth, and quiescent bacteria was therefore examined to gain insights for better designs. Of most significance, here, a study of the effect of the lead compound on the membrane, cell division, and associated proteins was performed to better understand the modes of action of this new semisynthetic glycopeptide antibiotic. The protein localization and morphological changes were evaluated upon treatment of *B. subtilis* producing GFP-MinD protein, *E. coli* producing various GFP-tagged cell division proteins and an

[a]*Antimicrobial Research Laboratory, New Chemistry Unit and School of Advanced Materials, Jawaharlal Nehru Centre for Advanced Scientific Research (JNCASR), Jakkur, Bengaluru, 560064, Karnataka, India. E-mail: jayanta@jncasr.ac.in; Tel: +91 802208 2565*

[b]*Department of Life Sciences, School of Natural Sciences, Shiv Nadar University, Dadri 201314, UP, India*

[c]*Applied Microbiology, Faculty of Biology and Biotechnology, Ruhr University Bochum, Universitätsstraße 150, 44780 Bochum, Germany*

† Electronic supplementary information (ESI) available. See DOI: https://doi.org/10.1039/d2sc05600c

amidase lacking mutant. Further, the potential of the lead compound as a preclinical candidate has been demonstrated in the murine thigh infection model against MRSA and chronic burn-wound infection against *A. baumannii*.

Results

Structure–activity relationship study

Design rationale. The second-generation glycopeptide antibiotics dalbavancin, oritavancin and possess hydrophobic moieties conjugated to the vancosamine sugar.[21–23] These antibiotics display improved activity against vancomycin-resistant bacteria. However, they are not active against Gram-negative bacteria. We had previously reported that the attachment of cationic lipophilic moieties onto the C-terminus of vancomycin results in interaction with the negatively charged bacterial membrane.[15] However, compounds with activity against both Gram-positive and Gram-negative bacteria were also slightly toxic. To address this, two sets of derivatives with C-terminus amido-alkyl-cationic (**1–5**) and aryl-cationic (**6–10**) substitutions were designed (Fig. 1A) and synthesized (Scheme S1†). The amphiphilicity of the cationic lipophilic moiety can be varied to selectively target the anionic bacterial membrane over the zwitterionic mammalian membrane. Biophysical studies and molecular dynamics simulation studies in polymeric and small molecular systems indicated that the inclusion of an amide spacer between the quaternary ammonium moiety and the hydrophobic moiety enhances the selectivity towards bacterial cells over mammalian cells.[24,25] The inclusion of an amide bond contributes to additional hydrogen bonding capacity to the bacterial lipids.[26] It was, therefore, envisioned that lipophilic cationic vancomycin derivatives with an amide spacer could result in improved selectivity towards bacteria.

Activity against Gram-positive bacteria. The antibacterial activity of vancomycin derivatives was determined as the lowest concentration required to completely inhibit bacterial growth (minimum inhibitory concentration, MIC). Against MRSA, the aryl-substituted derivatives **1–5** showed activity similar to vancomycin (Table 1). The increase in the carbon content of substituted moieties from six (**1**) to seven (**2** and **3**) to ten (**5**) to twelve (**4**), increased activity. Among these derivatives, the biphenyl-substituted, VanQbiph (**4**) was the most effective. It showed a 22 to 88-fold increase in activity as compared to vancomycin against VRSA. Against VRE, it showed a 40- to 60-fold enhancement in activity.

Among the amido-alkyl substituted compounds, **6–8** exhibited MICs similar to that of vancomycin against MRSA while the longer chain variants, **9** and **10** showed reduced activity. Against VRSA, the lower chain length variants, **6** and **7** were less effective; VanQAmC$_{10}$ (**8**) showed a significant 115–490-fold improvement in activity as compared to vancomycin. **9** and **10** had similar MICs and were slightly more effective than **8**. Against VRE, VanQAmC$_{10}$ (**8**) showed activity similar to that against VRSA (~160-fold improvement in activity as compared to vancomycin). In general, the series of amido-alkyl derivatives, **6–10** exhibited an increase in activity with longer chains, with no further enhancement in activity between longer chain substituted derivatives **9** and **10**. The amido-alkyl chain containing compounds exhibited better activity than those with aromatic substitutions. This indicated that the more flexible hydrophobic alkyl chain moieties resulted in better activity. VanQbiph (**4**), VanQAmC$_{10}$ (**8**), and VanQAmC$_{12}$ (**9**) demonstrate potency against vancomycin-resistant Gram-positive bacteria and were potential lead candidates. VanQAmC$_{10}$ shows activity similar to telavancin and is better than dalbavancin. The MIC of semi-synthetic glycopeptides such as oritavancin, telavancin and dalbavancin against VRE (VanA phenotype) were reported as 0.14 μM, 4 μM and 18 μM respectively.[4,20,41]

Activity against Gram-negative bacteria. While the aromatic hydrophobicity containing compounds **1–5** did not show significant activity, the alkyl-containing derivatives (**6–10**) were active against *A. baumannii* (Table 1). The activity against *P. aeruginosa* was strain-dependent, and the compounds were inactive against *K. pneumoniae*. Against *A. baumannii* (MTCC 1425 and AB R674), **6** and **7** were moderately active, while **8–10** showed improved activity with an MIC value of 6.3 μM. Against an MDR strain of *P. aeruginosa* **8–10** exhibited the highest activity. In general, compounds with higher hydrophobicity, **8–10**, displayed similar activity against Gram-negative bacteria. The results indicate that alkyl-cationic moieties are necessary for the antibacterial activity of vancomycin derivatives against Gram-negative bacteria. Of these, VanQAmC$_{10}$ (**8**) and VanQAmC$_{12}$ (**9**) demonstrated the highest activity against both Gram-positive and Gram-negative bacteria.

Hemolytic activity. To select the lead compounds, the toxicity of **1–10** was tested against human erythrocytes as their hemolytic activity (HC$_{50}$). The HC$_{50}$ is determined as the concentration at which 50% of the compound treated cells are lysed. The compounds with aromatic substitutions, **1–5**, possessed lower antibacterial activity and were also non-toxic (Table 1). The HC$_{50}$ for compounds **6–8** was also greater than 500 μM. Compounds **9** and **10** with longer chain length caused hemolysis. Based on the *in vitro* activity and hemolysis studies, VanQbiph (**4**) from the aryl-substituted compounds and VanQAmC$_{10}$ (**8**) from the alkyl-chain substituted compounds were selected for further investigations. VanQAmC$_{10}$ (**8**) was found to be non-toxic to MDCK cells with CC$_{50}$ >64 μM (Fig. S1†). VanQAmC$_{10}$ (**8**) was additionally non-toxic to RAW 264.7 cells up to 40 μM and was therefore taken forward *in vivo* investigation.[18]

Eradication of exponentially growing bacteria

To examine the antibacterial properties of the two leads, VanQbiph (**4**) and VanQAmC$_{10}$ (**8**), the kinetics of bactericidal activity against exponentially growing, log-phase cells of MRSA was evaluated (Fig. 1B). The minimum bactericidal concentration (MBC) of VanQbiph (**4**) and VanQAmC$_{10}$ (**8**) was at 2×MIC. VanQAmC$_{10}$ (**8**) showed faster killing than both VanQbiph (**4**) and vancomycin. At 2×MIC, both the compounds exhibited complete eradication in 24 h like vancomycin. At 8×MIC, VanQAmC$_{10}$ (**8**) showed complete eradication within 6 h while VanQbiph (**4**) showed a similar effect at 24 h. VanQAmC$_{10}$ (**8**)

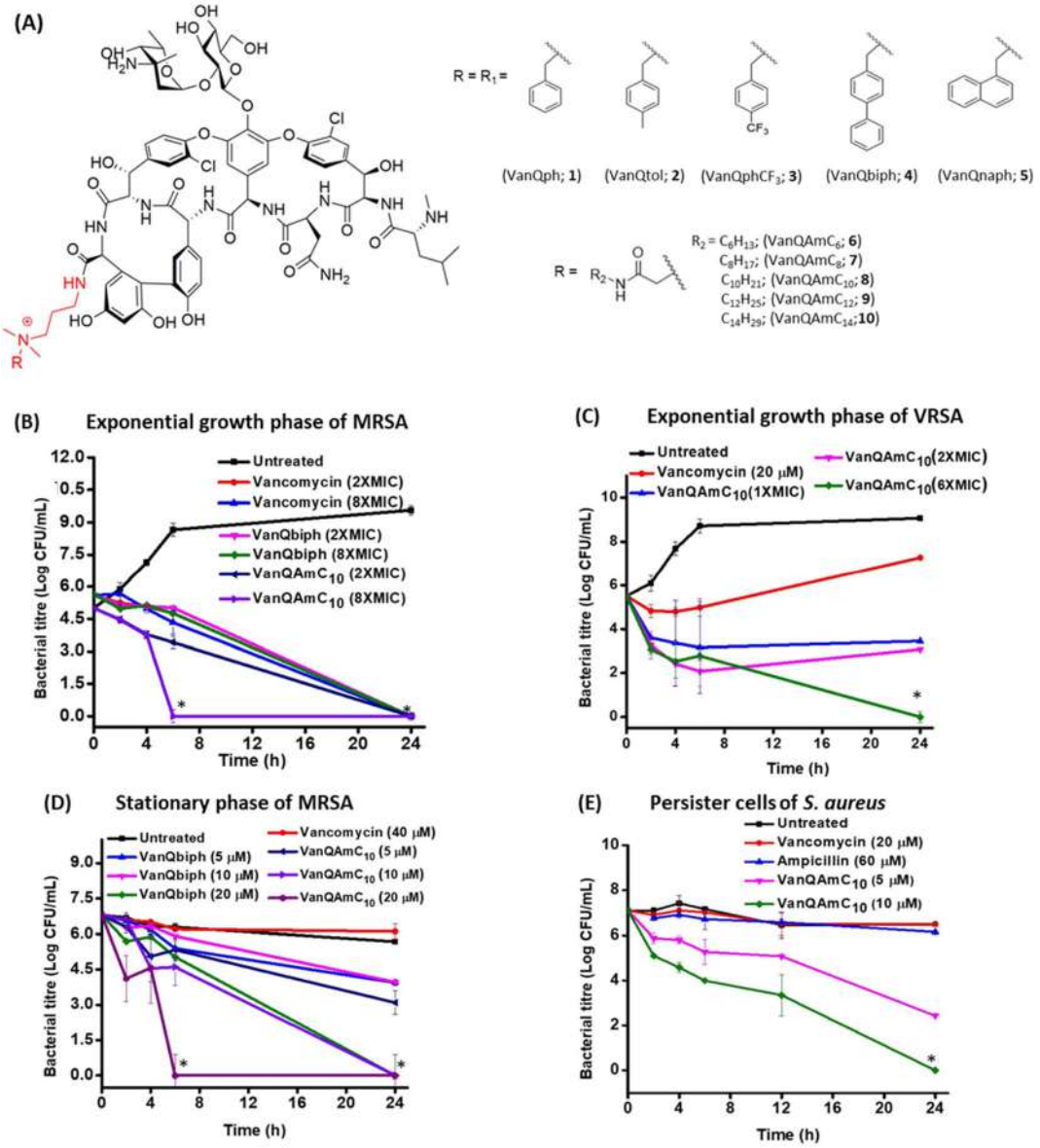

Fig. 1 (A) Structure of cationic lipophilic vancomycin derivatives. Bactericidal kinetics of (B) VanQbiph and $VanQAmC_{10}$ against exponential growth phase MRSA, (C) $VanQAmC_{10}$ against VRSA, (D) VanQbiph and $VanQAmC_{10}$ against stationary phase cells of MRSA, and (E) $VanQAmC_{10}$ against persister cells of *S. aureus*. Against MRSA, MIC of $VanQAmC_{10}$ = 0.4 μM, MIC of VanQbiph = 0.5 μM; MIC of $VanQAmC_{10}$ against VRSA = 1.6 μM and '*' indicates <50 CFU mL^{-1}.

showed a time and concentration-dependent activity while VanQbiph (**4**) and vancomycin showed only a time-dependent activity.

Against VRSA, $VanQAmC_{10}$ (**8**) exhibited better efficacy than VanQbiph (**4**) and was therefore tested for kinetics of killing. At MIC, it reduced the bacterial titer by 1.9 log CFU mL^{-1} in 24 h (Fig. 1C). At 2×MIC, an initial reduction was observed, followed by a 1 log CFU mL^{-1} increase in bacterial titer between 6 h and 24 h. At 6×MIC $VanQAmC_{10}$ resulted in complete eradication after 24 h. Treatment with vancomycin at 20 μM (sub-MIC), showed an initial growth inhibitory effect, followed by resumption of bacterial growth. Resistance in VRSA results from a combination of target modification as well as thickening of the cell wall. The additional mechanisms of $VanQAmC_{10}$ possibly contribute to its bactericidal activity against VRSA.

Eradication of metabolically inactive bacteria

The stationary phase cells and persister cells are metabolically repressed and phenotypically different from the log-phase cells.[27] For activity, the commonly used drugs, vancomycin, and linezolid require actively ongoing cellular processes. They are therefore ineffective against non-dividing bacteria. Even at the concentration of 40 μM, vancomycin did not reduce the number of viable stationary phase cells of MRSA in 24 h (Fig. 1D). The integrity of the bacterial membrane is imperative to survival irrespective of metabolic state. VanQbiph (**4**) and

Table 1 Antibacterial activity and hemolysis of vancomycin derivatives (**1–10**) against multi-drug-resistant Gram-positive and Gram-negative bacteria[a]

	Minimum inhibitory concentration (μM)									
	Gram-positive bacteria						Gram-negative bacteria			
Compound	MRSA	VRSA 1	VRSA 4	VRSA 12	VRE 51575	VRE 51559	AB 1425	PA R590	AB R674	HC_{50} (μM)
Vancomycin	0.6	345	345	345	750	250	100	100	100	N.D
VanQph (**1**)	1	>30	>30	>30	>30	>30	>30	>30	25.5	>500
VanQtol (**2**)	1	>30	16	>30	>30	>30	>30	>30	25.3	>500
VanQphCF$_3$ (**3**)	1	>30	15.8	>30	>30	>30	>30	24.6	24.6	>500
VanQbiph (**4**)	0.5	7.8	3.9	15.7	12.3	6.1	15.7	>30	24.5	>500
VanQnaph (**5**)	1	>30	3.9	>30	25	25	>30	>30	24.8	>500
VanQAmC$_6$ (**6**)	0.8	>30	6.3	>30	>30	25	25	12.5	12.5	>500
VanQAmC$_8$ (**7**)	0.8	3.1	3.1	>30	25	12.5	12.5	6.3	12.5	>500
VanQAmC$_{10}$ (**8**)	0.4	3.1	1.6–3.1	1.6	4	4	6.3	3.1	10	>500
VanQAmC$_{12}$ (**9**)	3.12	1.5	0.7	3	3.1	1.5	6.3	6.3	6.3	350
VanQAmC$_{14}$ (**10**)	6.25	3	1.5	3	3.1	1.5	6.3	6.3	12.5	150

[a] MRSA, methicillin-resistant *S. aureus* (ATCC 33591); VRSA, vancomycin-resistant *S. aureus*; VRE vancomycin-resistant *E. faecium* (VanA phenotype, ATCC 51559); vancomycin-resistant *E. faecalis* (VanB phenotype, ATCC 51575); ND, not determined. MIC against VRE and VRSA, HC_{50} of VanQAmC$_{10}$ was previously reported.[18]

VanQAmC$_{10}$ (**8**) were designed to incorporate membrane activity and therefore expected to be effective against the metabolically inactive cells of MRSA. VanQAmC$_{10}$ (**8**) showed better activity than VanQbiph (**4**) at the same concentration, similar to that observed against log-phase cells of MRSA. Irrespective of treatment concentration, VanQbiph (**4**), exhibited slow killing with no significant reduction in viability up to 6 h. Complete eradication was observed at a higher concentration of 20 μM in 24 h. VanQAmC$_{10}$ (**8**) showed rapid bactericidal activity that increased with concentration. It completely eradicated cells in 24 h at 10 μM and within 6 h at 20 μM.

Persister cells are a subpopulation of bacterial cultures that are refractory to antibiotic treatment.[28] Since VanQAmC$_{10}$ (**8**) was more effective than VanQbiph (**4**) against stationary phase cultures, its activity against persister cells was evaluated. VanQAmC$_{10}$ (**8**) exhibited a concentration-dependent bactericidal activity against the persister cells of MRSA (Fig. 1D). This activity was more rapid than that observed against stationary phase cells.

Another growing challenge in treating bacterial infections is the formation of biofilms, which are recalcitrant to antibiotic treatment.[29] Most antibiotics including vancomycin are rendered ineffective against biofilms consisting of both dividing and non-dividing cells, majorly due to their inability to penetrate through the extracellular polymeric matrix. Thus, it is important to develop compounds that eradicate biofilms as well as planktonic cells. Untreated biofilms of MRSA grew to a thickness of 11.8 μm (Fig. S3A†). The vancomycin-treated biofilms remained intact with thickness similar to the untreated control. VanQAmC$_{10}$ (**2**) was found to reduce the thickness of biofilms of MRSA by about 40%, showing a thickness of 7.4 μm as opposed to 11.8 and 10.1 μm for untreated and vancomycin treated cases respectively (Fig. S3B and C†).

Mechanism of action against Gram-positive bacteria

Membrane depolarisation. Having established the superior antibacterial properties of cationic lipophilic vancomycin derivatives, their modes of action were probed. The membrane disruption properties of both VanQbiph (**4**) and VanQAmC$_{10}$ (**8**) were studied to correlate the extent of membrane perturbation and bactericidal activity against both exponentially growing and non-growing bacterial cells. Their ability to depolarize the membrane was monitored using the fluorescent probe DiSC$_3$(5) (3,3′-dipropylthiadicarbocyanine iodide). DiSC$_3$(5) is sensitive to the membrane potential and as it accumulates in the membrane, the fluorescence intensity decreases due to self-quenching. Upon dissipation of membrane potential, an increase in fluorescence is observed due to DiSC$_3$(5) being dispersed in the solution. Against *B. subtilis* and MRSA, both the compounds VanQbiph (**4**) and VanQAmC$_{10}$ (**8**) depolarised the membrane within 2 minutes post-treatment at 10 μM (Fig. 2A and B). The depolarization occurred in a concentration-dependent manner (Fig. S2A†). The alkyl chain substituted compound, VanQAmC$_{10}$ (**8**) showed a higher extent of depolarisation than the aromatic biphenyl substituted, VanQbiph (**4**). Against stationary phase cells of MRSA also, rapid dissipation of membrane potential was observed within 2 minutes post-treatment with both VanQbiph (**4**) and VanQAmC$_{10}$ (**8**) (Fig. 2C). Vancomycin did not affect the membrane potential.

Membrane permeabilization. The kinetics of permeabilization of membranes of MRSA and *B. subtilis* by the compounds was measured by the uptake of propidium iodide (PI). The dye, PI does not permeate through intact membranes. When the membrane integrity is compromised, it enters the cell and fluoresces upon binding to the DNA. Both VanQbiph (**4**) and VanQAmC$_{10}$ (**8**) permeabilized the membrane in a concentration-dependent manner (Fig. S2†). While vancomycin does not affect the membrane integrity, VanQAmC$_{10}$ (**8**) exhibited rapid permeabilization within 4 minutes of treatment. VanQbiph (**4**)

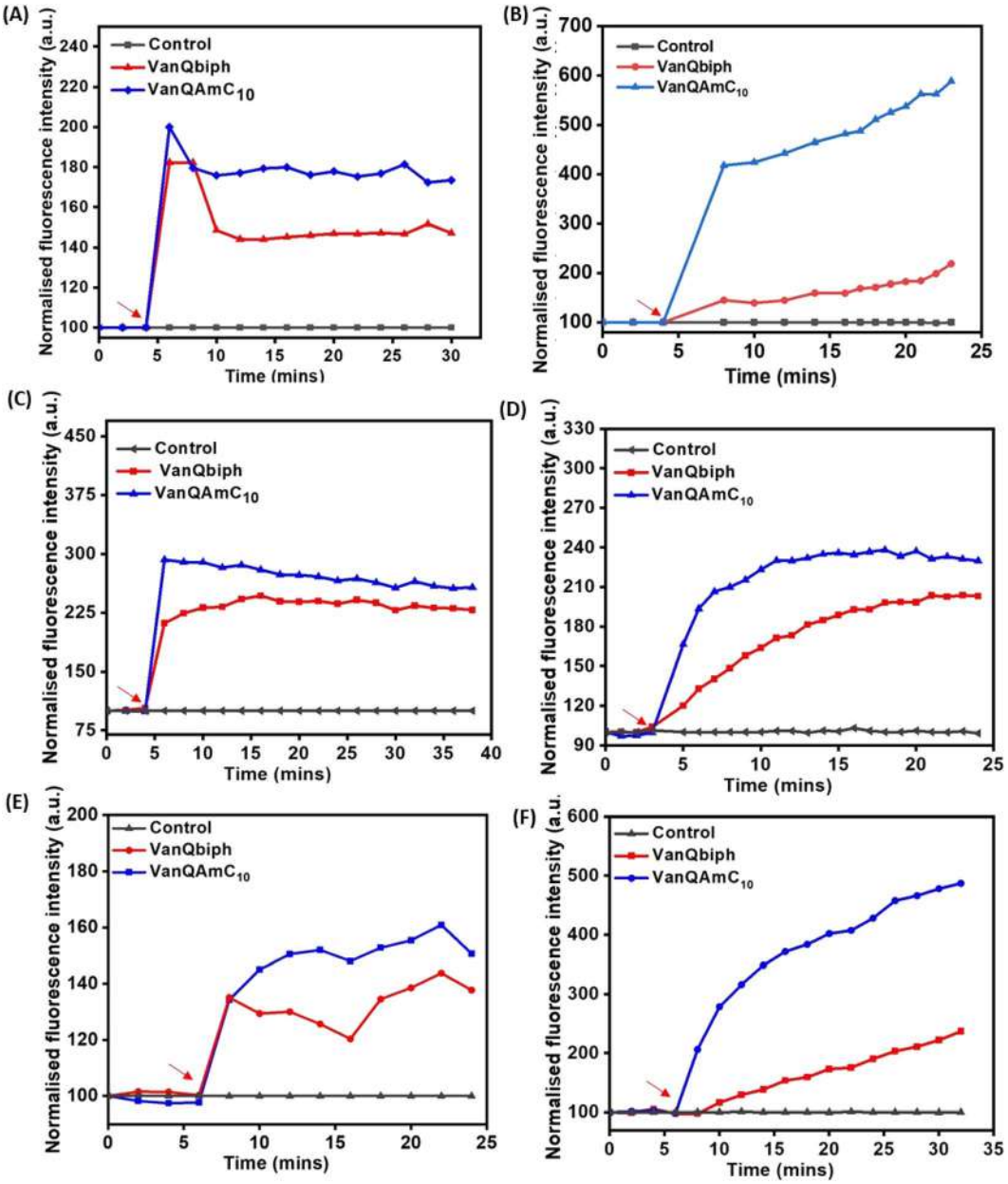

Fig. 2 Membrane–perturbation properties of VanQbiph and $VanQAmC_{10}$. Membrane depolarization against, (A) exponentially growing MRSA, (B) exponentially growing *B. subtilis*, upon treatment at 10 μM, and (C) stationary phase cells of MRSA upon treatment at 20 μM. Membrane permeabilization against, (D) exponentially growing MRSA, (E) exponentially growing *B. subtilis*, upon treatment at 10 μM, and (F) stationary phase cells of MRSA upon treatment at 20 μM. Red arrows indicate compound addition. The error percentage between replicates of an experiment was lesser than 5%. The images are representative of results from three independent experiments.

showed slower permeabilization (Fig. 2D and E). They caused gradual permeabilization against the stationary phase cells of MRSA as well (Fig. 2F). The extent of permeabilization was higher for $VanQAmC_{10}$ (**8**) than VanQbiph (**4**) against both the log-phase and stationary-phase bacteria similar to that observed during depolarisation. Membrane-perturbation may be the predominant mechanism leading to the antibacterial activity against metabolically inactive bacteria.

To confirm that membrane perturbation contributed to cell death, the bacterial viability was evaluated under conditions similar to the mechanistic studies. A decrease in the number of viable cells was observed with an increase in the concentration of both VanQbiph (**4**) and $VanQAmC_{10}$ (**8**) (Fig. 3A). The number of viable cells was lower upon treatment with $VanQAmC_{10}$ (**8**) than when treated with VanQbiph (**4**) at the same concentration. At 5 μM and 10 μM, VanQbiph (**4**) showed 0.8 log CFU mL^{-1} and 2.2 log CFU mL^{-1} reduction respectively. $VanQAmC_{10}$ (**8**) showed 2 log CFU mL^{-1} and 4 log CFU mL^{-1} reduction upon treatment at 5 μM and 10 μM respectively. Treatment with both the compounds at 20 μM resulted in complete eradication of the

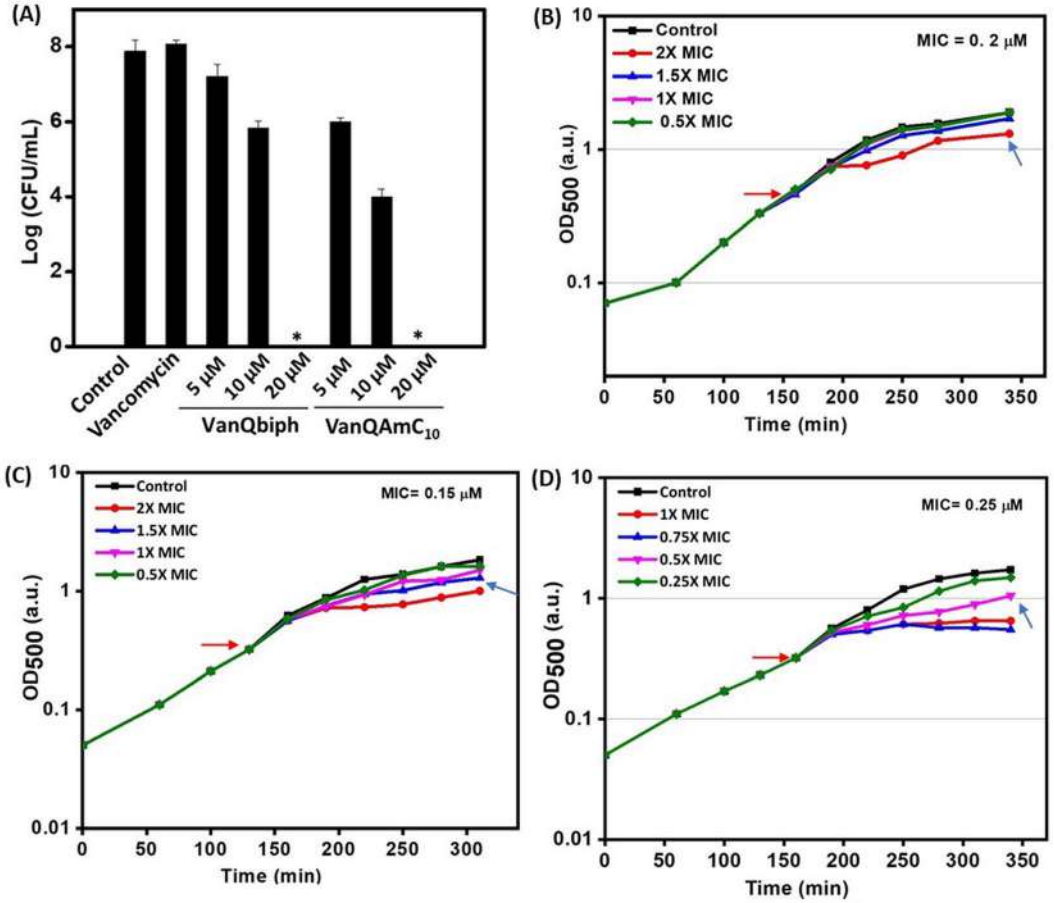

Fig. 3 (A) Viability of planktonic cells post-treatment in HEPES-glucose; acute growth retardation upon treatment with (B) vancomycin, (C) VanQbiph, (D) $VanQAmC_{10}$. '*' indicates <50 CFU mL^{-1}. Red arrow indicates compound addition and blue arrow indicates PEC.

bacteria. Vancomycin did not reduce the viability of bacteria even at 40 μM, under the same conditions. The stronger membrane–perturbation properties of $VanQAmC_{10}$ (**8**) therefore contribute to higher activity against both exponentially growing and stationary phase bacteria.

Acute effect on bacterial growth. The mechanisms of action in Gram-positive bacteria were further examined in the model bacterium *B. subtilis*. The study of the mechanism of action of a drug requires live cells under antibiotic stress. A 30–50% growth inhibition upon treatment, triggers a stress response in the bacterial cell while allowing cell proliferation to progress at a level sufficient to study the effect of the compound. The lowest concentration at which this effect was observed, was termed the physiologically effective concentration (PEC). The MIC of vancomycin, VanQbiph (**4**), and $VanQAmC_{10}$ (**8**) against *B. subtilis* were 0.2 μM, 0.15 μM, and 0.25 μM, respectively. The acute effect of different antibiotic concentrations on exponentially growing bacterial cultures were tested to identify the PEC (Fig. 3B–D). Vancomycin showed growth retardation at 0.4 μM. Similar growth retardation was observed at lower concentrations for both compounds. $VanQAmC_{10}$ (**8**) showed an inhibitory effect from 0.125 μM, while VanQbiph (**4**) showed a similar inhibition effect from 0.2 μM. The presence of cationic lipophilic moieties possibly result in higher accumulation in the membrane region leading to growth inhibition at lower concentrations.

Cell wall biosynthesis inhibition. To further study the mechanisms contributing to the growth retardation, microscopic studies were carried out upon treatment of *B. subtilis* with compounds. Upon inhibition of cell wall biosynthesis, holes are formed in the peptidoglycan layer where new cell wall material is no longer incorporated. The cytoplasmic membrane extrudes out of these perforations, appearing as bubbles on the cell surface when treated with a 1 : 3 mixture of acetic acid and methanol.[30] This phenomenon is exhibited by compounds that inhibit cell wall biosyntheses like vancomycin and not agents that only perturb the membrane integrity such as gramicidin-A and valinomycin.[31] Like vancomycin, VanQbiph (**4**) and $VanQAmC_{10}$ (**8**) showed bubbles on the surface, indicating that they inhibit cell wall biosynthesis and compromise the integrity of the cell wall (Fig. 4A).

MinD delocalization. MinD is a peripheral membrane protein that localizes at the cell poles and is part of the cell division regulation machinery. It has been reported that treatment with membrane-depolarizing agents like valinomycin results in the delocalization of the protein which appears in

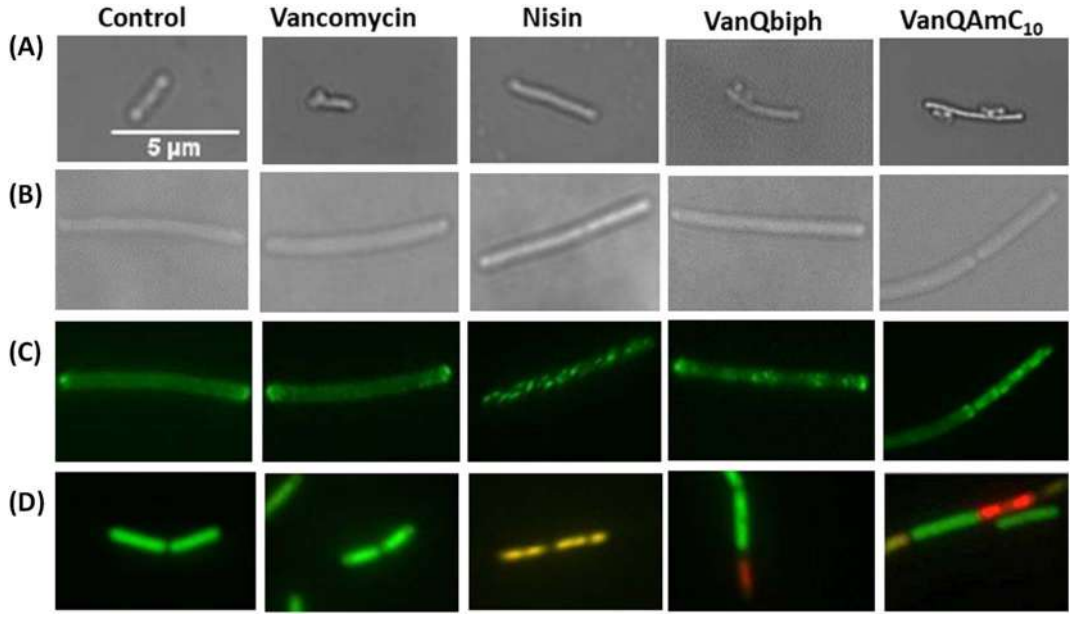

Fig. 4 Examination of the effect of VanQbiph, $VanQAmC_{10}$, vancomycin and nisin on cell membrane and wall integrity of *B. subtilis* upon treatment at respective PECs. (A) Inhibition of cell wall biosynthesis and compromise of cell wall integrity by visualization of 'bubbles' on the bacterial surface post acetic acid/methanol fixation through light microscopy; (B) light microscopy to assess the morphology of GFP-MinD expressing *B. subtilis* cells; (C) delocalization of GFP-MinD through fluorescence microscopy; (D) membrane permeabilization and pore formation monitored through fluorescence with the BacLight bacterial viability kit. Scale of all images is the same (5 μm).

irregularly distributed spots throughout the cell. Since the compounds depolarise the bacterial membrane, their effect on the localization of the GFP-tagged MinD protein of *B. subtilis* was investigated. Treatment with VanQbiph (**4**) and $VanQAmC_{10}$ (**8**) at the PEC resulted in an irregular distribution of GFP-labelled MinD across the cells (Fig. 4B and C). This indicates that the compound also possibly stalls the bacterial cell division process.

Membrane permeabilization without pore formation. To examine if the compounds form pores on the membrane, a mixture of the fluorescent dyes SYTO 9 and PI was used. While SYTO 9 penetrates both intact and permeabilized cells staining them green, PI is unable to cross the intact membrane and stains only permeabilized or dead cells red. Membrane-disrupting antibiotics such as nisin are known to form pores in the membrane is stained by both SYTO 9 and PI (Fig. 4D). However, upon treatment with VanQbiph (**4**) and $VanQAmC_{10}$ (**8**), cells did not co-stain cells with both the dyes, indicating non-specific interaction with the membrane. Around 20% of the cells visualized post-treatment with both compounds were stained by PI and therefore permeabilized.

Antagonization assay with *N*,*N*′-diacetyl-L-Lys–D-Ala–D-Ala (Ac_2KAA) and teichoic acid. Ac_2KAA can act as a competitive ligand to the target of glycopeptide antibiotics and therefore antagonize antibacterial activity. In the presence of 500 μM of Ac_2KAA, the activity of $VanQAmC_{10}$ (**8**) was reduced by 2-fold. However, the MIC of vancomycin increased from 0.6 μM to >30 μM (>40-fold increase in MIC) in presence of the same amount of Ac_2KAA. The 2-fold reduction in the activity of $VanQAmC_{10}$ (**8**) accounts for the loss of activity due to D-Ala–D-Ala binding. This implied that it acted through additional mechanisms that are independent of Ala-D-Ala binding. The presence of the positive charge in $VanQAmC_{10}$ (**8**) could result in interactions with the negatively charged components of the bacterial cell wall like teichoic acid. C-terminal trimethyl ammonium modified vancomycin derivative has been reported to bind to teichoic acid.[32] However, no change in the MIC of both vancomycin and $VanQAmC_{10}$ was observed in presence of lipoteichoic acid as a competing ligand, implying that it was not a target.

Mechanism of action in Gram-negative bacteria (*E. coli*)

Lysis of *E. coli*. The MIC of $VanQAmC_{10}$ (**8**) against *E. coli* was 16 μM whereas vancomycin was inactive up to 66 μM. Microscopic examination of *E. coli* treated with $VanQAmC_{10}$ at 25 μM, showed that it completely lysed the cells, while vancomycin did not affect the cells (Fig. 5A). Over 240 minutes, *E. coli* treated with $VanQAmC_{10}$ (at 25 μM), gradually grow bulky before finally lysing (ESI Video†). It punctured the cell, causing the cytoplasm to leak out as extrusions on the surface of the bacteria after which the cells flattened and disintegrated. Previous studies in Gram-negative bacteria indicated that $VanQAmC_{10}$ (**8**) can depolarise and permeabilize their outer and inner membrane.[18]

Effect on bacterial cell division. The division process broadly involves the following stages, (i) marking of the division site; (ii) employing the divisome and constriction of the cell wall through activation of cell wall synthesis; (iii) membrane fusion and cell wall hydrolysis for compartmentalization and physical separation into daughter cells.[33] It was envisioned that the membrane–perturbation properties of $VanQAmC_{10}$ (**8**) could affect bacterial cell division and the localization of associated

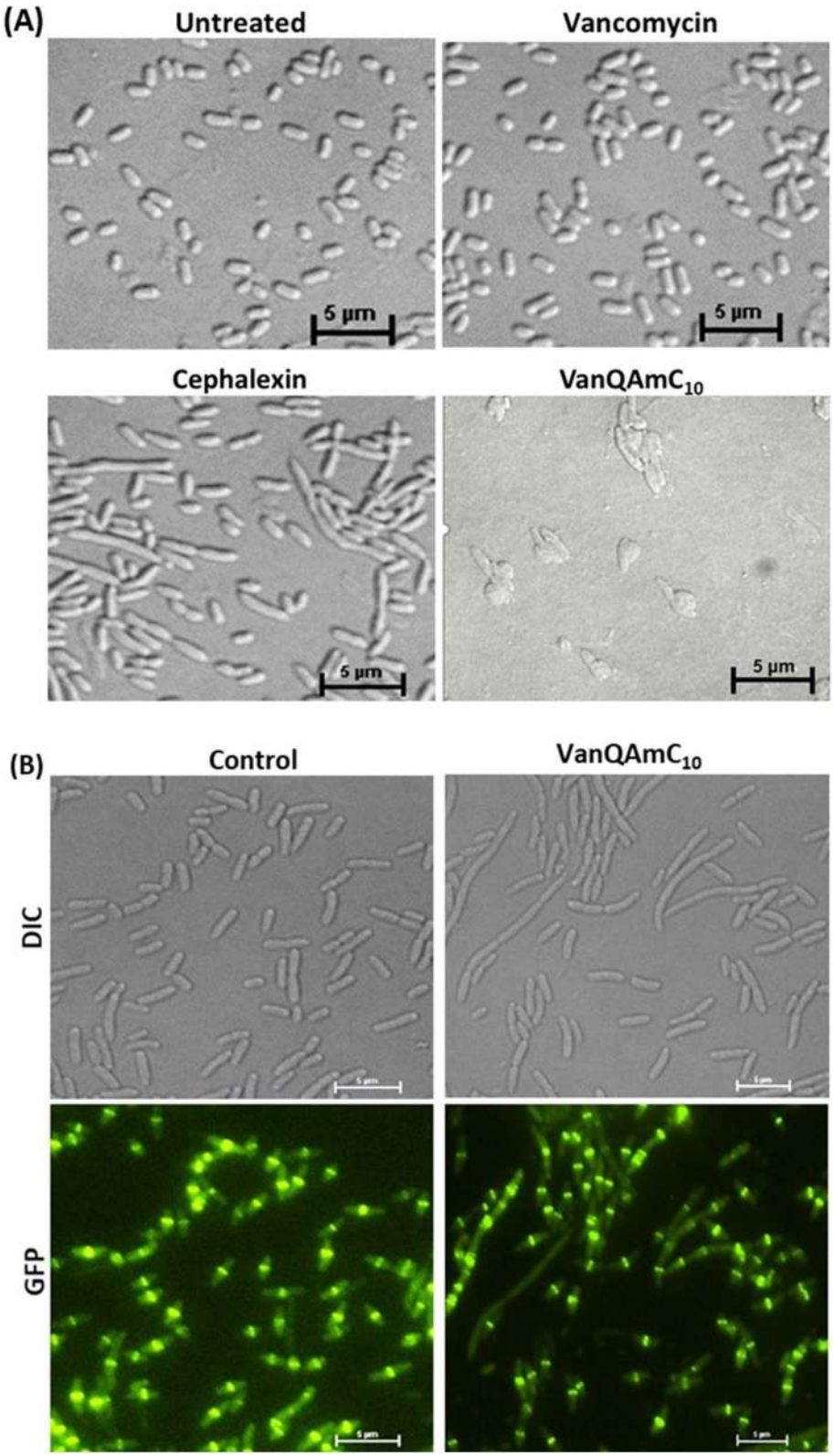

Fig. 5 Examination of E. coli cells treated with vancomycin, cephalexin and VanQAmC10 to study the effect on bacterial membrane integrity and cell division. (A) Light microscopy of wild-type E. coli upon treatment with vancomycin (34 μM), and VanQAmC10 (25 μM); (B) light and fluorescence microscopy in GFP-FtsZ expressing E. coli to assess morphological changes and localization of FtsZ post-treatment with VanQAmC10 (15 μM) for 40 min; (C) delocalization of GFP-FtsI in GFP-FtsI expressing E. coli through fluorescence microscopy and morphological changes through light microscopy upon treatment with vancomycin (34 μM), cephalexin (22 μM) and VanQAmC10 (10 μM); (D) light microscopy to assess morphological changes in E. coli MG1655 Δ*amiAC* mutant, when untreated and treated with vancomycin (3 μM) and VanQAmC10 (2 μM). Black arrows indicate morphological aberrations.

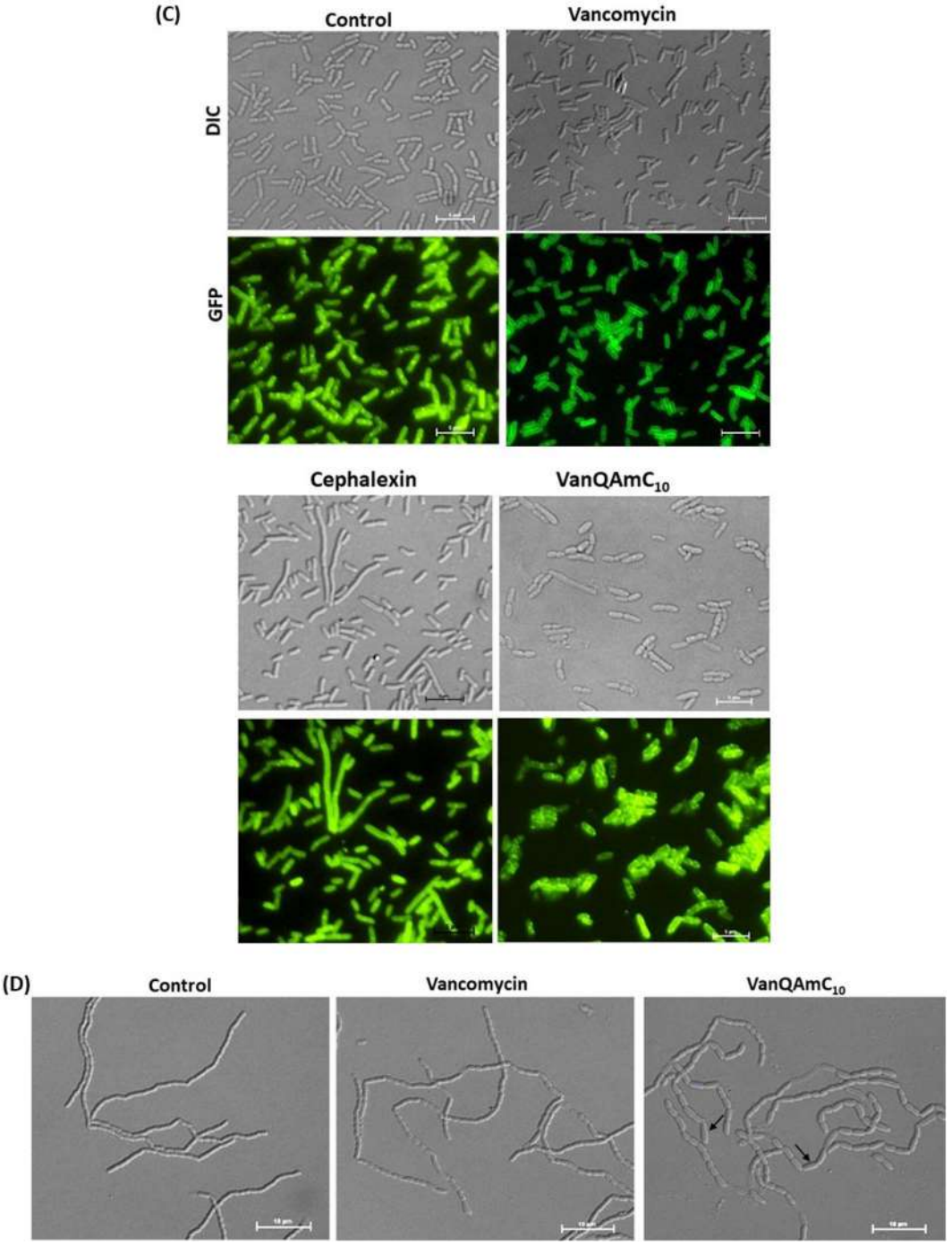

Fig. 5 (*contd.*)

proteins. Its effect on the various stages of cell division was investigated. In the first stage of cell division in bacteria, the particular localization of FtsZ at the septum is crucial. The effect of antibiotic treatment on localization and morphology against GFP-FtsZ producing bacteria was therefore first inspected.

Inhibition of cell division in GFP-FtsZ producing *E. coli*. The FtsZ protein assembles into a membrane-associated ring structure at the division septum. It recruits other proteins for the progression and completion of cell division.[34] The effect of $VanQAmC_{10}$ on the localization of FtsZ and morphology in *E. coli* producing green fluorescent protein (GFP)-tagged FtsZ was studied through microscopy (Fig. 5B). The cells were treated with IPTG to overexpress *gfp-ftsZ* and then either treated with compounds or left untreated. Upon treatment with 15 μM of $VanQAmC_{10}$, the cells appear to be filamentous with variable lengths of up to 4 μm, while cells in the control group were ~2.5 μm long. Incubation with $VanQAmC_{10}$ for a longer time (130 minutes) results in bulkier filamentous cells, with severely

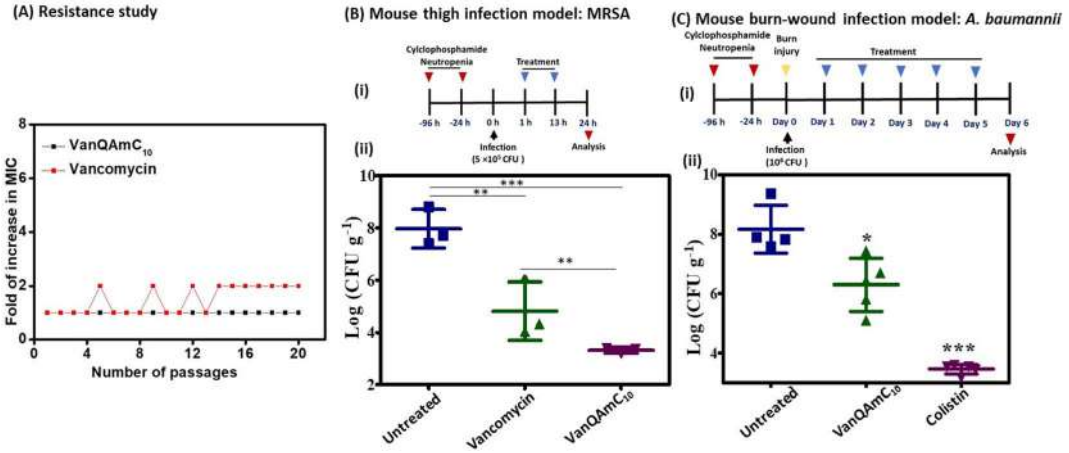

Fig. 6 (A) Propensity of vancomycin and $VanQAmC_{10}$ to induce resistance in MRSA upon serial exposure to sub-MIC concentrations; (B) (i) experimental design for *in vivo* efficacy study in a murine thigh infection model, (ii) *in vivo* efficacy of $VanQAmC_{10}$ and vancomycin against the multidrug-resistant methicillin-resistant *S. aureus* (MRSA) (n = 3/dose). Antibiotics were administered intraperitoneally twice at 12 h intervals at a dose of 12 mg kg^{-1}. (C) (i) Experimental design for *in vivo* efficacy study in murine burn wound infection model, (ii) *in vivo* efficacy of $VanQAmC_{10}$ and colistin against the carbapenem-resistant *A. baumannii* (n = 5/dose, 1 mouse died in untreated control). $VanQAmC_{10}$ and colistin were treated topically at 30 mg kg^{-1} for 5 days ('***' indicates $p < 0.0001$, '**' indicates $p < 0.001$, '*' $p < 0.05$, $p = 0.08$ (n.s.) for $VanQAmC_{10}$ with respect to vancomycin).

distorted shapes (Fig. S4†). However, the localization and distribution of Z-rings remain unaltered. IPTG-treated cells formed minicells of ~1.5 μm length, which is characteristic of cells overproducing FtsZ.[35] Known inhibitors of FtsZ alter the regular midcell distribution of Z-rings.[36] The results indicate that $VanQAmC_{10}$ either affects FtsZ differently than the known inhibitors or that it inhibits bacterial cell division indirectly.

Mislocalization of GFP-FtsI protein. FtsI or PBP-3 is the only transpeptidase required for bacterial cell division and localizes to the septal ring.[37] It regulates the degree of cross-linking and coordinates the division process. GFP-tagged FtsI producing *E. coli* cells were treated with vancomycin (at 34 μM) and $VanQAmC_{10}$ (at 10 μM and 15 μM; Fig. 5C) and then examined under the microscope. The untreated and vancomycin-treated cells showed green fluorescence due to the localization of FtsI at the septum. Cephalexin, a known inhibitor of FtsI, induces a filamentous phenotype with mislocalized GFP-FtsI protein.[38] Upon treatment with 10 μM of $VanQAmC_{10}$, larger phenotypes of variable sizes are observed with shape defects. Some cells appear filamentous like in the case of cephalexin. The GFP-FtsI protein appears as green fluorescent spots delocalized across the cell in 60% of the cells visualized. At a higher concentration of 15 μM, bulkier cells with more distorted shapes than those at 10 μM were observed (Fig. S5†). Thus, $VanQAmC_{10}$ mislocalizes the cell division protein, FtsI, and inhibits further cell division.

Sensitivity against mutants lacking AmiA and AmiC. The bacterial amidases help cleave the septum in the final stage of cell division to produce daughter cells.[39] In the absence of amidases, chains of unseparated cells are formed (Fig. 5D). These retain distinct cytoplasmic compartments but share an outer membrane.[39] These cells are known to be hypersensitive to antibiotics and detergents. However, Δ*amiAC* mutations are resistant to killing by cephalexin.[38] The MIC of $VanQAmC_{10}$ against the Δ*amiAC* mutant was reduced to 4 μM, while that of vancomycin was >10 μM. This indicates that $VanQAmC_{10}$ inhibits cell division through mechanisms different from cephalexin. Microscopic examination of the mutants treated with sub-inhibitory concentrations of $VanQAmC_{10}$ revealed larger cell phenotypes of variable sizes. This is indicative of impaired cell division. Cell debris due to lysis after compound treatment are also visible. In the vancomycin-treated cells, few cells appear larger and bulky while most appear similar to the untreated bacteria (Fig. 5D).

In vivo activity of $VanQAmC_{10}$

Resistance induction. Having observed the multiple mechanisms of $VanQAmC_{10}$, the potential as a preclinical candidate was examined. The multimodal mechanisms possibly lead to the lack of resistance development to $VanQAmC_{10}$ in MRSA after 20 passages, while vancomycin showed a 2-fold increase in MIC (Fig. 6A). Additionally, $VanQAmC_{10}$ does not induce resistance in *A. baumannii*, unlike colistin.[18] The frequency of resistance for both vancomycin and $VanQAmC_{10}$ against MRSA was $<10^{-8}$ indicating the absence of spontaneous mutants.

Activity in mouse liver homogenate and human plasma. The MIC of $VanQAmC_{10}$ against MRSA and VRE remained unchanged in both plasma as well as liver homogenate, thereby confirming their stability for activity *in vivo* (Table S1†).

Efficacy in mouse infection models. The LD_{50} of $VanQAmC_{10}$ (**8**) was found to be 70 mg kg^{-1} through intravenous injection.[18] When administered intraperitoneally, a 130 mg kg^{-1} dose was found to be well tolerated and all mice survived. The LD_{50} of $VanQAmC_{10}$ was greater than 160 mg kg^{-1} when administered subcutaneously. The *in vitro* activity, low toxicity, and stability in plasma and liver homogenate, supported the potential of $VanQAmC_{10}$ as a candidate for the treatment of bacterial infections. The efficacy of $VanQAmC_{10}$ (**8**) against MRSA was

tested in a neutropenic mouse thigh infection model. Infection was established by injecting them with 5×10^5 CFU of MRSA in the thigh. 1 h and 13 h post-infection, mice were treated with 12 mg kg^{-1} of vancomycin and $VanQAmC_{10}$ administered intraperitoneally (Fig. 6B). The mice were sacrificed 24 h post-infection. The pre-treatment bacterial load was found to be 6.3 log CFU mL^{-1}. In the untreated group, the bacterial load increased to 8 log CFU g^{-1}. The vancomycin treated group showed a bacterial load of 4.8 log CFU g^{-1} of tissue. However, treatment with $VanQAmC_{10}$ reduced the bacterial load to 3.3 log CFU g^{-1}, which is a 1.5 log CFU g^{-1} lower bacterial load than observed against vancomycin. The results highlight the superior *in vivo* efficacy of $VanQAmC_{10}$ as compared to that of the parent drug vancomycin.

Further, the efficacy of $VanQAmC_{10}$ (**8**) was tested in a chronic burn-wound infection model of *A. baumannii*.[40] Chronic burn wounds on the back of mice were infected with *A. baumannii*. 24 h post-infection, before initiation of treatment, the bacterial load was found to be 7.5 log CFU g^{-1}. Infected mice were treated with 30 mg kg^{-1} of $VanQAmC_{10}$ and colistin for five days consecutively. The bacterial load in the untreated group increased to 8 log CFU g^{-1} six days post-infection. Treatment with $VanQAmC_{10}$ resulted in a 2.2 log CFU g^{-1} lower bacterial load as compared to the untreated mice, while colistin showed a 4.8 log CFU g^{-1} load lower bacterial load as compared to the untreated mice at the same dose (Fig. 6C). The use of colistin is however limited due to its toxicity and bacteria easily develop resistance to it. Therefore, $VanQAmC_{10}$ presents a promising alternative for both Gram-positive and Gram-negative bacteria.

Discussion

Vancomycin served as a life-saving drug against MDR Gram-positive bacterial infections for over thirty years until the report of resistance. This makes it an attractive drug for further development against the escalating incidences of resistant bacteria. The more difficult to treat Gram-negative bacteria are inherently resistant to vancomycin. We have shown that the conjugation of cationic lipophilic moieties to vancomycin results in broad-spectrum activity against both Gram-negative bacteria and Gram-positive bacteria. The cationic lipophilic moiety incorporates interaction with the negatively charged bacterial membrane, therefore, perturbing membrane integrity. Through comparison of alkyl and aryl-substituted derivatives, $VanQAmC_{10}$ and VanQbiph respectively, we demonstrate that the alkyl substitutions exhibit better membrane activity as well as bactericidal activity against both metabolically active and inactive bacteria (Fig. 1). Vancomycin, on the other hand, is ineffective against the metabolically inactive bacterial cells. The lead compound, $VanQAmC_{10}$ shows remarkable improvement in antibacterial efficacy in a mouse thigh infection model as compared to vancomycin against MRSA (Fig. 6). It was also effective against burn wound infections in mice caused by *A. baumannii*.

Scientific interest toward membrane-active vancomycin derivatives has been growing due to their ability to overcome both inherited and non-inherited resistance.[3] Therefore, a holistic understanding of how membrane-active vancomycin derivatives affect the bacteria would be imperative for the further development of new agents. In a step toward this, we used a variety of biological assays to provide new insights into the mechanism of action of $VanQAmC_{10}$. It acts through mechanisms in addition to cell wall synthesis inhibition by binding to the D-Ala–D-Ala terminus which is known for the parent drug, vancomycin. To rule out the secondary effects as a result of cell death, mechanisms of action were studied at sub-inhibitory concentrations. Systematic investigations in *B. subtilis* revealed that it acts by simultaneously, (i) inhibiting cell wall biosynthesis, (ii) permeabilizing cells through non-specific interactions with membrane, and (iii) dissipation of membrane-potential leading to delocalization of the cell division protein, MinD (Fig. 4). The dissipation of membrane potential by $VanQAmC_{10}$ possibly results in malfunctioning of the bacterial cell division machinery.[42] To comprehend how $VanQAmC_{10}$ affects Gram-negative bacteria, studies were conducted on the model Gram-negative bacterium, *E. coli*. Treatment with $VanQAmC_{10}$ results in the lysis of the cells and therefore cell death. Treatment of the various strains of *E. coli* (wild-type, GFP-FtsI, GFP-FtsZ, and Δ*amiAC*) at subinhibitory concentrations resulted in cells of variable sizes and distorted morphology (Fig. 5). It did not impede the formation of the Z-ring in the first stage of cell division. It delocalized the FtsI protein required for the synthesis of the cell wall during septum formation in the second stage of cell division. Mutants lacking AmiA and AmiC enzymes were more sensitive to $VanQAmC_{10}$ which is consistent with reports that these mutants have increased susceptibility to surfactants. These confirm that $VanQAmC_{10}$ inhibits cell division at sub-inhibitory concentrations through mechanisms different from the FtsZ inhibitors and the β-lactam, cephalexin. Our findings suggest that the membrane perturbing properties of $VanQAmC_{10}$ affect the localization of proteins involved in cell division, leading to severe cell wall and membrane defects. This possibly ultimately leads to a breach in the cell membrane and cell death.

Overall, here we demonstrate a new vancomycin derivative, $VanQAmC_{10}$ which is highly effective against Gram-positive as well as Gram-negative bacteria both *in vitro* and *in vivo*. The multiple mechanisms of action contribute to the negligible resistance induction and superior antibacterial properties of $VanQAmC_{10}$ as compared to the parent drug. It represents a new class of multi-target, multi-effect glycopeptide antibiotics. The findings augment a new dimension to the understanding of the mechanism of such membrane-active glycopeptide derivatives.

Data availability

The datasets supporting this article have been uploaded as part of the ESI.The ESI† includes materials and methods; experimental protocols for *in vitro* microbiological assays (activity, biofilms, time-kill kinetics, and mechanistic studies) and toxicity, and *in vivo* activity and toxicity; supplementary figures; details of characterization of intermediates and final compounds through ^{1}H NMR, IR, and HR-MS.

Author contributions

PS, project design, synthesis, characterisation, performing *in vitro* microbiological assays (activity and mechanistic studies) and *in vivo* infection studies, data curation, formal analysis, manuscript writing and editing; KD, synthesis and characterisation; GD, cytotoxicity testing and *in vivo* activity studies, manuscript editing; JEB, experimental design and analysis for mechanisms of action against *B. subtilis*, manuscript editing; MM and RP, experimental design and analysis for mechanisms of action against *E. coli*, manuscript editing; JH, project design, research supervision, manuscript writing and editing.

Conflicts of interest

There are no conflicts to declare.

Acknowledgements

We acknowledge DST-DAAD bilateral cooperation project (INT/FRG/DAAD/P-15/2018) and JNCASR for funding. We thank Dr Sandip Samaddar (JNCASR), Dr Riya Mukherjee (JNCASR) and Pascal Dietze (RUB) for excellent technical support and scientific discussions. We thank Dr Chandradhish Ghosh and Dr Venkateswarlu Yarlagadda for fruitful scientific discussions. RP acknowledges funding from CSIR (37(1701)/17/EMR-II) and Shiv Nadar University. MM acknowledges support by DST Inspire fellowship. JEB acknowledges funding from the DAAD Program DST 2018 (57389759). We thank Dr Sidharth Chopra (Central Drug Research Institute, Lucknow) for the gift of drug-resistant clinical isolates.

References

1 **https://www.who.int/foodsafety/cia/en/**, 2019.
2 E. Binda, F. Marinelli and G. L. Marcone, *Antibiotics*, 2014, **3**, 572–594.
3 G. Dhanda, P. Sarkar, S. Samaddar and J. Haldar, *J. Med. Chem.*, 2019, **62**, 3184–3205.
4 D. Zeng, D. Debabov, T. L. Hartsell, R. J. Cano, S. Adams, J. A. Schuyler, R. McMillan and J. L. Pace, *Cold Spring Harb Perspect. Med.*, 2016, **6**, a026989.
5 M. A. T. Blaskovich, K. A. Hansford, M. S. Butler, Z. Jia, A. E. Mark and M. A. Cooper, *ACS Infect. Dis.*, 2018, **4**, 715–735.
6 A. Okano, N. A. Isley and D. L. Boger, *Proc. Natl. Acad. Sci. U. S. A.*, 2017, **114**, E5052–E5061.
7 V. Yarlagadda, P. Sarkar, G. B. Manjunath and J. Haldar, *Bioorg. Med. Chem. Lett.*, 2015, **25**, 5477–5480.
8 V. Yarlagadda, P. Sarkar, S. Samaddar and J. Haldar, *Angew. Chem., Int. Ed. Engl.*, 2016, **55**, 7836–7840.
9 D. Guan, F. Chen, Y. Qiu, B. Jiang, L. Gong, L. Lan and W. Huang, *Angew. Chem., Int. Ed. Engl.*, 2019, **58**, 6678–6682.
10 A. Antonoplis, X. Zang, M. A. Huttner, K. K. L. Chong, Y. B. Lee, J. Y. Co, M. R. Amieva, K. A. Kline, P. A. Wender and L. Cegelski, *J. Am. Chem. Soc.*, 2018, **140**, 16140–16151.
11 M. M. Fernandes, K. Ivanova, J. Hoyo, S. Perez-Rafael, A. Francesko and T. Tzanov, *ACS Appl. Mater. Interfaces*, 2017, **9**, 15022–15030.
12 V. Yarlagadda, P. Sarkar, S. Samaddar, G. B. Manjunath, S. D. Mitra, K. Paramanandham, B. R. Shome and J. Haldar, *ACS Infect. Dis.*, 2018, **4**, 1093–1101.
13 A. Antonoplis, X. Zang, T. Wegner, P. A. Wender and L. Cegelski, *ACS Chem. Biol.*, 2019, **14**, 2065–2070.
14 E. van Groesen, C. J. Slingerland, P. Innocenti, M. Mihajlovic, R. Masereeuw and N. I. Martin, *ACS Infect. Dis.*, 2021, **7**, 2746–2754.
15 E. Lei, H. Tao, S. Jiao, A. Yang, Y. Zhou, M. Wang, K. Wen, Y. Wang, Z. Chen, X. Chen, J. Song, C. Zhou, W. Huang, L. Xu, D. Guan, C. Tan, H. Liu, Q. Cai, K. Zhou, J. Modica, S. Y. Huang, W. Huang and X. Feng, *J. Am. Chem. Soc.*, 2022, **144**, 10622–10639.
16 R. E. Impey, D. A. Hawkins, J. M. Sutton and T. P. Soares da Costa, *Antibiotics*, 2020, **9**.
17 M. A. T. Blaskovich, K. A. Hansford, Y. Gong, M. S. Butler, C. Muldoon, J. X. Huang, S. Ramu, A. B. Silva, M. Cheng, A. M. Kavanagh, Z. Ziora, R. Premraj, F. Lindahl, T. A. Bradford, J. C. Lee, T. Karoli, R. Pelingon, D. J. Edwards, M. Amado, A. G. Elliott, W. Phetsang, N. H. Daud, J. E. Deecke, H. E. Sidjabat, S. Ramaologa, J. Zuegg, J. R. Betley, A. P. G. Beevers, R. A. G. Smith, J. A. Roberts, D. L. Paterson and M. A. Cooper, *Nat. Commun.*, 2018, **9**, 22.
18 P. Sarkar, S. Samaddar, V. Ammanathan, V. Yarlagadda, C. Ghosh, M. Shukla, G. Kaul, R. Manjithaya, S. Chopra and J. Haldar, *ACS Chem. Biol.*, 2020, **15**, 884–889.
19 V. Yarlagadda, G. B. Manjunath, P. Sarkar, P. Akkapeddi, K. Paramanandham, B. R. Shome, R. Ravikumar and J. Haldar, *ACS Infect. Dis.*, 2016, **2**, 132–139.
20 V. Yarlagadda, P. Akkapeddi, G. B. Manjunath and J. Haldar, *J. Med. Chem.*, 2014, **57**, 4558–4568.
21 J. A. Karlowsky, K. Nichol and G. G. Zhanel, *Clin. Infect. Dis.*, 2015, **61**(Suppl 2), S58–S68.
22 M. T. Guskey and B. T. Tsuji, *Pharmacotherapy*, 2010, **30**, 80–94.
23 G. G. Zhanel, D. Calic, F. Schweizer, S. Zelenitsky, H. Adam, P. R. Lagace-Wiens, E. Rubinstein, A. S. Gin, D. J. Hoban and J. A. Karlowsky, *Drugs*, 2010, **70**, 859–886.
24 D. S. Uppu, P. Akkapeddi, G. B. Manjunath, V. Yarlagadda, J. Hoque and J. Haldar, *Chem. Comm.*, 2013, **49**, 9389–9391.
25 J. Hoque, S. Gonuguntla, V. Yarlagadda, V. K. Aswal and J. Haldar, *Phys. Chem. Chem. Phys.*, 2014, **16**, 11279–11288.
26 D. S. S. M. Uppu, M. M. Konai, U. Baul, P. Singh, T. K. Siersma, S. Samaddar, S. Vemparala, L. W. Hamoen, C. Narayana and J. Haldar, *Chem. Sci.*, 2016, **7**, 4613–4623.
27 X. Zhou and L. Cegelski, *Biochemistry*, 2012, **51**, 8143–8153.
28 I. Keren, N. Kaldalu, A. Spoering, Y. Wang and K. Lewis, *FEMS Microbiol. Lett.*, 2004, **230**, 13–18.
29 D. E. Moormeier and K. W. Bayles, *Mol. Microbiol.*, 2017, **104**, 365–376.
30 T. Schneider, T. Kruse, R. Wimmer, I. Wiedemann, V. Sass, U. Pag, A. Jansen, A. K. Nielsen, P. H. Mygind, D. S. Raventos, S. Neve, B. Ravn, A. M. Bonvin, L. De

Maria, A. S. Andersen, L. K. Gammelgaard, H. G. Sahl and H. H. Kristensen, *Science*, 2010, **328**, 1168–1172.
31 M. Wenzel, B. Kohl, D. Munch, N. Raatschen, H. B. Albada, L. Hamoen, N. Metzler-Nolte, H. G. Sahl and J. E. Bandow, *Antimicrob. Agents Chemother.*, 2012, **56**, 5749–5757.
32 Z. C. Wu, N. A. Isley, A. Okano, W. J. Weiss and D. L. Boger, *J. Org. Chem.*, 2020, **85**, 1365–1375.
33 L. I. Rothfield and S. S. Justice, *Cell*, 1997, **88**, 581–584.
34 W. Margolin, *Nat. Rev. Mol. Cell Biol.*, 2005, **6**, 862–871.
35 J. E. Ward Jr and J. Lutkenhaus, *Cell*, 1985, **42**, 941–949.
36 L. Araujo-Bazan, L. B. Ruiz-Avila, D. Andreu, S. Huecas and J. M. Andreu, *Front. Microbiol.*, 2016, **7**, 1558.
37 M. C. Wissel and D. S. Weiss, *J. Bacteriol.*, 2004, **186**, 490–502.
38 H. S. Chung, Z. Yao, N. W. Goehring, R. Kishony, J. Beckwith and D. Kahne, *Proc. Natl. Acad. Sci. U. S. A.*, 2009, **106**, 21872–21877.
39 R. Priyadarshini, M. A. de Pedro and K. D. Young, *J. Bacteriol.*, 2007, **189**, 5334–5347.
40 M. G. Thompson, C. C. Black, R. L. Pavlicek, C. L. Honnold, M. C. Wise, Y. A. Alamneh, J. K. Moon, J. L. Kessler, Y. Si, R. Williams, S. Yildirim, B. C. Kirkup Jr, R. K. Green, E. R. Hall, T. J. Palys and D. V. Zurawski, *Antimicrob. Agents Chemother.*, 2014, **58**, 1332–1342.
41 J. M. Streit, *Diagn. Microbiol. Infect. Dis.*, 2004, **48**, 137–143.
42 P. Sarkar, *J. Med. Chem.*, 2021, 10185.

Chemical Science

ROYAL SOCIETY OF CHEMISTRY

EDGE ARTICLE

View Article Online
View Journal | View Issue

Cite this: *Chem. Sci.*, 2024, **15**, 259

All publication charges for this article have been paid for by the Royal Society of Chemistry

Received 28th September 2023
Accepted 12th November 2023

DOI: 10.1039/d3sc05124b

rsc.li/chemical-science

Small molecular adjuvants repurpose antibiotics towards Gram-negative bacterial infections and multispecies bacterial biofilms†

Rajib Dey,[a] Sudip Mukherjee,[a] Riya Mukherjee[a] and Jayanta Haldar *[ab]

Gram-negative bacterial infections pose a significant challenge due to two major resistance elements, including the impermeability of the outer membrane and the overexpression of efflux pumps, which contribute to antibiotic resistance. Additionally, the coexistence of multispecies superbugs in mixed species biofilms further complicates treatment, as these infections are refractory to most antibiotics. To address this issue, combining obsolete antibiotics with non-antibiotic adjuvants that target bacterial membranes has shown promise in combating antibacterial resistance. However, the clinical translation of this cocktail therapy has been hindered by the toxicity associated with these membrane active adjuvants, mainly due to a limited understanding of their structure and mechanism of action. Towards this goal, herein, we have designed a small molecular adjuvant by tuning different structural parameters, such as the balance between hydrophilic and hydrophobic groups, spatial positioning of hydrophobicity and hydrogen bonding interactions, causing moderate membrane perturbation in bacterial cells without any toxicity to mammalian cells. Moderate membrane perturbation not only enhances the internalization of antibiotics, but also increases the intracellular concentration of drugs by hampering the efflux machinery. This revitalises the efficacy of various classes of antibiotics by 32–512 fold, without inducing toxicity. The leading combination not only exhibits potent bactericidal activity against *A. baumannii* biofilms but also effectively disrupts mature multispecies biofilms composed of *A. baumannii* and methicillin-resistant *Staphylococcus aureus* (MRSA), which is typically resistant to most antibiotics. Importantly, the combination therapy demonstrates good biocompatibility and excellent *in vivo* antibacterial efficacy (>99% reduction) in a skin infection model of *A. baumannii*. Interestingly, *A. baumannii* shows reduced susceptibility to develop resistance against the leading combination, underscoring its potential for treating multi-drug resistant infections.

Introduction

The increasing incidence of infectious diseases and the associated mortality caused by drug-resistant infections have created a significant concern in public healthcare.[1,2] A recent report indicates that approximately 5 million people succumb to drug-resistant infections, with a majority of these infections caused by Gram-negative superbugs, such as carbapenem-resistant *A. baumannii*, *P. aeruginosa*, and Enterobacteriaceae spp., which have been designated as critical priority pathogens by the World Health Organization (WHO).[3] The emergence of these life-threatening pathogens in both community-associated and hospital-acquired infections has posed a serious challenge to the healthcare system.[4] The prevalence of multispecies bacterial co-infections and secondary bacterial infections among hospitalized COVID patients has further exacerbated the situation.[5,6] This menace is amplified by the slow pace of development, approval, and translation of novel antibiotics, rendering these infections resilient to almost all existing antibiotic classes and demanding innovative alternatives. Resistance mechanisms in Gram-negative bacteria are broadly classified into: (1) impermeability caused by the outer membrane consisting of lipopolysaccharides (LPSs); (2) overexpression of efflux pumps driven by membrane potential; (3) production of antibiotic degrading enzymes such as β-lactamases (including serine-β-lactamase and metallo-β-lactamase); and (4) target mutations.[7] Among these, impermeability of the outer membrane and the transmembrane efflux pumps contribute to multi-drug resistance in Gram-negative pathogens, rendering most conventional antibiotics ineffective.[8] Recently, membrane-targeting antibiotic adjuvants have

[a]*Antimicrobial Research Laboratory, New Chemistry Unit, Jawaharlal Nehru Centre for Advanced Scientific Research, Jakkur, Bengaluru 560064, Karnataka, India. E-mail: jayanta@jncasr.ac.in*

[b]*School of Advanced Materials, Jawaharlal Nehru Centre for Advanced Scientific Research, Jakkur, Bengaluru 560064, Karnataka, India*

† Electronic supplementary information (ESI) available: Experimental section, supplementary figures for characterization and biological assays. See DOI: https://doi.org/10.1039/d3sc05124b

emerged as a promising strategy to tackle antimicrobial resistance (AMR) by repurposing and revitalizing obsolete antibiotics.[9–12] Many of these adjuvants draw inspiration from naturally occurring antimicrobial peptides (AMPs).[13,14] These cationic amphiphilic peptides, which directly target bacterial membranes, not only exhibit direct microbicidal action but also enhance the intracellular concentration of antibiotics, acting as potentiators.[15,16]

However, the current use of cationic lipophilic compounds as permeabilization enhancers to sensitize resistant antibiotics is hindered by their toxicity towards mammalian cells.[17,18] Therefore, a detailed understanding of the optimal amphiphilicity in the structure such as the balance between hydrophobicity and hydrophilic moieties, spatial positioning of hydrophobic groups and the influence of hydrogen bonding on structural parameters, is crucial.[19–21] Furthermore, the overexpression of efflux machinery

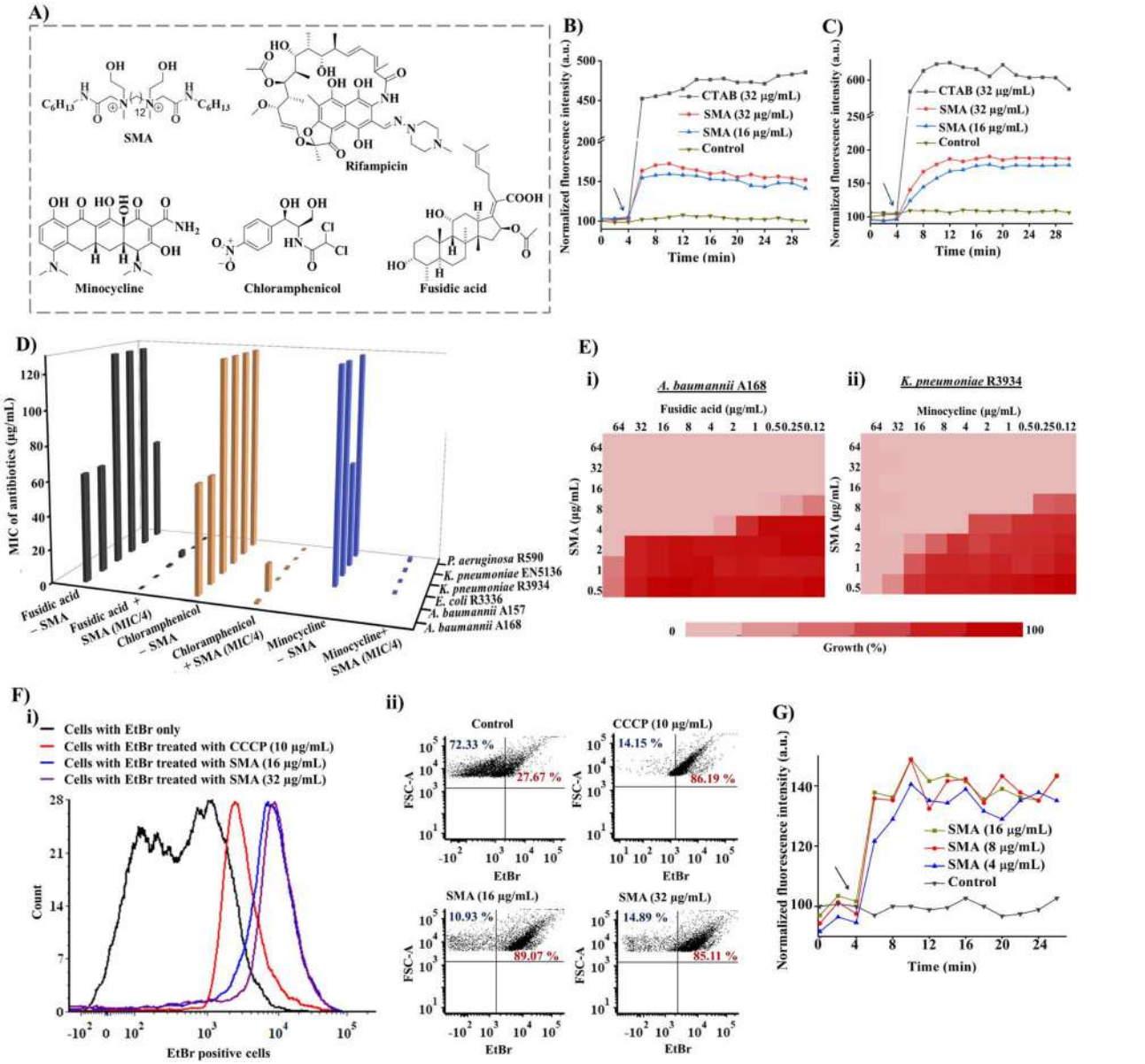

Fig. 1 (A) Chemical structures of SMA and resistant antibiotics sensitized by the adjuvant; (B) outer membrane permeabilization (by using *N*-phenyl-1-naphthylamine (NPN) fluorescent dye); and (C) cytoplasmic membrane depolarization (by using a $DiSC_3(5)$ fluorescence probe) by SMA at different sub-MIC concentrations against NDM-1 producing bacteria *A. baumannii* A168. Surfactant CTAB (cetyltrimethylammonium bromide) was taken as a positive control. Arrow indicates the time of compound addition; (D) 3D flow chart representing the potentiation efficacy of SMA with fusidic acid, chloramphenicol, and minocycline against various drug-resistant Gram-negative superbugs; (E) chequerboard assay revealing synergistic efficacy of (i) SMA and fusidic acid against *A. baumannii* A168, (ii) SMA and minocycline against *K. pneumoniae* R3934; (F) efflux pump inhibition assay; (i) the number of parent cells used in the EtBr assay; (ii) SMA activated a dose-dependent increase in ethidium bromide (EtBr) accumulation in *A. baumannii* A168 bacteria. Carbonyl cyanide 3-chlorophenylhydrazone (CCCP) was taken as a positive control. Fluorescence intensity was measured using a flow cytometer; (G) minocycline uptake assay upon treatment with different concentrations of SMA against NDM-1 producing *K. pneumoniae* R3934.

is another major cause of acquired resistance to antibiotics.[22,23] While several effective efflux pump disruptors have been reported, their severe toxicity has limited their applicability as antibiotic adjuvants.[24,25] A detailed understanding of the structural parameters and mechanistic insights of these membrane potential-targeting compounds is scarce in the literature. In the last two decades, different small molecular mimics of antimicrobial peptides (SMAMPs) have been developed as antibiotic adjuvants to repurpose and rejuvenate obsolete antibiotics. As examples, SPR741 (developed by Spero Therapeutics) and Nylexa (developed by NovaBiotics) are in the initial stage of clinical trials to be used as potentiators with a wide range of antibiotics.[26,27] Recently, another three drugs approved for non-antimicrobial indications, namely 5-fluorouracil, fluspirilene, and Bay 11-7082, resensitized a clinical strain of *A. baumannii* to azithromycin.[28]

In this study, we investigated the synergistic activity of a small molecular adjuvant to repurpose and revitalize different resistant antibiotics including rifampicin, fusidic acid, minocycline and chloramphenicol against Gram-negative pathogens (Fig. 1A). The structural features of the compound were designed to obtain a weak to moderate membrane-perturbing and membrane-depolarizing adjuvant without inducing toxicity towards mammalian cells. The adjuvant enhances the intracellular concentration of antibiotics, and the synergistic effect was validated through checkerboard assays against various multi-drug resistant Gram-negative bacteria and their clinical isolates. The bactericidal activities of the leading combinations were investigated against NDM-1 producing pathogens using time-kill kinetics. The biocompatibility of the leading combinations and the small molecule alone were assessed against mammalian cell lines and through *in vivo* systemic toxicity, respectively. Furthermore, the efficiency of the leading combination in disrupting preformed biofilms was studied. In addition to biofilm-mediated infections, multispecies bacterial infections pose an intense threat to healthcare practices. Multispecies biofilms are prevalent in nature and are particularly prominent in dental abscesses, cystic fibrosis, and diabetic wounds. Therefore, the antibacterial and anti-biofilm efficacy of the small molecular adjuvant-based combination therapy was evaluated against a co-culture and biofilm of MRSA and NDM-1 producing *A. baumannii*, which represents a multispecies bacterial infection. Importantly, the *in vivo* antibacterial activity of the leading combination therapy was investigated using a mouse model of skin infection caused by NDM-1 producing Gram-negative pathogens. Finally, the frequency of resistance development for the combination was assessed.

Results and discussion

Design and synthesis of small molecular adjuvant (SMA)

The small molecular adjuvant, SMA, was carefully designed to incorporate specific structural features that enhance its interaction with the lipid bilayer of Gram-negative bacteria. The presence of the outer membrane in these bacteria creates an additional barrier that restricts the permeability of antibiotics. To overcome this challenge, hexyl pendant long chains with spacer hydrophobicity were introduced in the molecular design. The strategic distribution of hydrophobic moieties in both the spacer and pendent regions was fine-tuned in our previous study, as the spatial positioning of hydrophobicity plays a crucial role in improving the selectivity of membrane-targeting compounds.[15,21] In addition, two ethanol moieties were introduced to achieve optimal amphiphilicity and to facilitate superior interaction with the outer membrane of Gram-negative bacteria through hydrogen bonding. The rational design of SMA considered these structural parameters to ensure its effectiveness as a membrane-targeting adjuvant. The synthesis of SMA was performed on a large scale (gram scale) using a straightforward three-step synthetic route, as outlined in Scheme S1.† Detailed synthetic procedures can be found in the ESI (Fig. S1–S3),† providing comprehensive information on the synthesis of SMA.

Overall, the design and synthesis of SMA involved careful consideration of hydrophobicity, spatial positioning of hydrophobic groups, and the incorporation of ethanol moieties to achieve optimal amphiphilicity and facilitate effective interaction with the outer membrane of Gram-negative bacteria.

Membrane targeting mechanism of SMA against Gram-negative bacteria

The initial exploration of SMA's limited antibacterial activity against Gram-negative superbugs prompted us to investigate its potential to enhance the efficiency of resistant antibiotics against multi-drug resistant Gram-negative strains. To unravel the mechanism of SMA's interaction with bacterial membranes, we conducted membrane depolarization and bacterial outer membrane permeabilization assays on Gram-negative bacteria.

The bacterial membrane potential is reliant on the proton-motive force (PMF), which comprises two components: *trans*-membrane electrical potential ($\Delta\Psi$) and *trans*-membrane pH gradient (ΔpH).[29] We assessed bacterial membrane depolarization using the fluorescent dye 3,3′ dipropylthiadicarbocyanine iodide ($DiSC_3(5)$). In energized cells, this dye accumulates at the cytoplasmic membrane and undergoes self-quenching, resulting in low fluorescence intensity. However, if the bacterial membrane potential is disrupted, the dye is released into the extracellular environment, leading to an increase in fluorescence intensity. Additionally, we evaluated the outer membrane permeabilization using *N*-phenyl-1-naphthylamine (NPN). Since NPN cannot penetrate the lipopolysaccharide (LPS) layer, it cannot enter the bacterial phospholipid layer under normal conditions. However, in a perturbed membrane, NPN readily translocates into the bacterial phospholipid layer, resulting in an escalation of fluorescence intensity. We employed the $DiSC_3(5)$ assay and NPN assay to investigate the extent of membrane-perturbing properties of the SMA compound against *A. baumannii* A168 bacteria (Fig. 1B and C). As a positive control, we used the surfactant CTAB, which exhibited strong outer membrane permeabilization, evident from a sharp increase in fluorescence intensity. In contrast, treatment with SMA resulted in a slight increase in fluorescence intensity in the NPN assay, indicating moderate outer membrane permeabilization against *A. baumannii* A168. Similarly, SMA induced moderate

cytoplasmic membrane depolarization compared to CTAB in the $DiSC_3(5)$ assay. Overall, SMA, a small amphiphilic molecule, demonstrated a modest membrane-perturbing nature, which can aid in potentiation of antibiotics that are unable to cross the outer membrane or are expelled by efflux pumps.

These findings shed light on the membrane targeting mechanism of SMA and its potential to facilitate the action of antibiotics by perturbing the bacterial membrane, allowing the entry of otherwise restricted antibiotics and overcoming efflux pump-mediated resistance.

In vitro potentiation ability against drug-resistant Gram-negative superbugs

To assess the *in vitro* synergistic activity of SMA with various resistant antibiotics, we conducted chequerboard assays against a range of multi-drug resistant Gram-negative bacteria, including New Delhi metallo-β-lactamase-1 (NDM-1) producing strains. Initially, we determined the minimum inhibitory concentrations (MICs) of SMA and the antibiotics against the tested pathogens. SMA exhibited limited activity against most Gram-negative pathogens, with MIC values ranging from 64–256 μg mL^{-1}, except for the *A. baumannii* A157 strain, where it displayed an MIC of 16 μg mL^{-1}. The relatively poor activity of SMA may be attributed to its moderate membrane-perturbing nature.

Next, we evaluated the potentiation ability of SMA against multi-drug resistant Gram-negative superbugs, (including NDM-1 producing strains, through chequerboard assays with four different classes of antibiotics: rifampicin, minocycline, chloramphenicol, and fusidic acid (Fig. 1D and Table 1)). Rifampicin and fusidic acid, both hydrophobic antibiotics

Table 1 Potentiation efficacy of SMA with obsolete antibiotics against Gram-negative bacteria

Bacterial strain	SMA MIC (μg mL^{-1})	Antibiotic MIC (μg mL^{-1})	MIC of antibiotic (μg mL^{-1}) in the presence of SMA			FICI[a]
			MIC/4	MIC/8	MIC/16	
Rifampicin						
A. baumannii R674	128	64	0.25	0.25	1	0.08–0.25
A. baumannii A168	256	16	0.031	0.031	0.062	0.05–0.25
A. baumannii A157	16	1	0.031	0.062	0.5	0.16–0.31
E. coli R3336	256	512	0.125	0.25	1	0.05–0.25
K. pneumoniae R3934	128	512	0.25	0.25	1	0.06–0.25
K. pneumoniae ATCC BAA2146	64	16	0.125	0.5	ND[b]	0.16–0.26
K. pneumoniae EN5136	64	8	0.125	0.5	2	0.27–0.31
P. aeruginosa R590	128	128	0.125	0.125	0.125	0.06–0.25
Fusidic acid						
A. baumannii R674	128	64	ND	ND	ND	ND
A. baumannii A168	256	64	0.125	0.125	0.5	0.08–0.13
A. baumannii A157	16	64	0.25	2	16	0.16–0.31
E. coli R3336	256	>512	1	8	ND	0.14–0.25
K. pneumoniae R3934	128	512	4	16	ND	0.26–0.38
K. pneumoniae ATCC BAA2146	64	>256	0.125	ND	ND	0.25–0.31
K. pneumoniae EN5136	64	>256	0.125	2	32	0.14–0.25
P. aeruginosa R590	128	64	0.5	4	ND	0.19–0.26
Chloramphenicol						
A. baumannii R674	128	>128	ND	ND	ND	ND
A. baumannii A168	256	64	1	8	16	0.25–0.31
A. baumannii A157	16	64	16	32	ND	0.5–0.51
E. coli R3336	256	>128	0.125	0.25	1	0.14–0.25
K. pneumoniae R3934	128	>128	1	4	ND	0.16–0.31
K. pneumoniae ATCC BAA2146	64	>256	0.125	64	ND	0.25–0.37
K. pneumoniae EN5136	64	>256	0.125	32	ND	0.38–0.51
P. aeruginosa R590	128	>128	1	4	ND	0.25–0.35
Minocycline						
A. baumannii R674	128	8	0.125	0.25	1	0.19–0.31
A. baumannii A168	256	ND	ND	ND	ND	ND
A. baumannii A157	16	ND	ND	ND	ND	ND
E. coli R3336	256	32	0.125	0.125	0.5	0.08–0.19
K. pneumoniae R3934	128	64	0.125	0.5	4	0.09–0.13
K. pneumoniae ATCC BAA2146	64	16	0.125	1	16	0.19–0.26
K. pneumoniae EN5136	64	16	0.125	0.5	1	0.13–0.26
P. aeruginosa R590	128	8	1	4	8	0.38–0.56

[a] FICI – Fractional inhibitory concentration index (determined at $MIC_{SMA}/16$ to $MIC_{SMA}/4$). [b] ND – not determined.

commonly used for treating tuberculosis and Gram-positive infections, respectively, are typically impermeable to the Gram-negative bacterial outer membrane due to the presence of LPSs.[30] Conversely, bacteria have developed resistance against other antibiotics such as minocycline and chloramphenicol through the efflux pump mechanism (*e.g.*, TetA and AcrAB-TolC) present in the cytoplasmic membrane.[31] SMA demonstrated the ability to potentiate these four antibiotics against various multidrug-resistant Gram-negative superbugs.

SMA significantly reduced the MIC values of rifampicin by 32-2024-fold at its sub-MIC concentration against all tested Gram-negative bacteria, indicating its potential for repurposing this anti-tuberculosis antibiotic (Table 1, Fig. S4†). Notably, SMA sensitized fusidic acid, commonly prescribed for treating Gram-positive bacterial infections, against drug-resistant Gram-negative bacteria, with a fractional inhibitory concentration index (FICI) value of <0.4. In the case of NDM-1 producing bacterium *E. coli* R3336, the combination therapy reduced the MIC of fusidic acid by 512-fold. Against another NDM-1 producing pathogen *A. baumannii* A168, the combination of SMA at an MIC/8 concentration lowered the MIC of fusidic acid to 0.125 μg mL^{-1} (512-fold reduction) (Fig. 1D, E(i), and S5†).

Furthermore, SMA showed promising synergy with chloramphenicol, reducing the MIC values of the antibiotic by 4-512-fold against most tested pathogens (Table 1, Fig. 1D and S6†). In the case of the NDM-1 producing bacteria *K. pneumoniae* R3934 strain, the combination of SMA at an MIC/8 concentration and chloramphenicol resulted in a MIC reduction to 4 μg mL^{-1} (Fig. 1D). However, SMA only exhibited an additive effect with chloramphenicol against the *A. baumannii* A157 strain, with a FICI value >0.5. Additionally, SMA sensitized minocycline by reducing the MIC values to ≤1 μg mL^{-1}, with an FICI value of <0.5, against the tested Gram-negative pathogens (Table 1 and Fig. 1D). Specifically, SMA at an MIC/8 concentration decreased the MIC value of minocycline to 0.5 μg mL^{-1} (by 128-fold reduction) and 1 μg mL^{-1} (16-fold reduction) against NDM-1 producing bacteria *K. pneumoniae* R3934 and *K. pneumoniae* BAAATCC2146, respectively (Table 1, Fig. 1E(ii), S7†). In summary, our findings validate that SMA can potentiate rifampicin and fusidic acid and restore the efficacy of minocycline and chloramphenicol against critical drug-resistant Gram-negative bacteria, leveraging its membrane-active nature. These results reinforce our initial premise and underscore the potential of SMA as an adjunct therapy to combat drug-resistant Gram-negative superbugs.

Inhibition of efflux pumps

Bacterial efflux pumps play a significant role in the rapid emergence of drug resistance, with many of these pumps located in the cytoplasmic membrane, such as the resistance-nodulation-cell division (RND) superfamily and major facilitator superfamily (MFS), which are regulated by membrane potential.[22] Given that SMA exhibited a moderate membrane depolarization effect, resulting in a change in membrane potential, we investigated its direct impact on bacterial efflux pumps.

To assess the efflux inhibition properties of SMA, we performed an ethidium bromide (EtBr) accumulation assay using flow cytometry in *A. baumannii* A168 (NDM-1+). EtBr is a substrate of the RND efflux machinery and is expelled from healthy bacterial cells.[32] Carbonyl cyanide 3-chlorophenylhydrazone (CCCP) was taken as a positive control, which abolishes the entire proton-motive force resulting in the disruption of efflux machinery, while cells stained with EtBr only served as the negative control. CCCP at 10 μg mL^{-1} directly inhibited the efflux pump and increased the intracellular concentration of EtBr. Similarly, our potentiator SMA, at different concentrations (16 μg mL^{-1} and 32 μg mL^{-1}), significantly increased the number of EtBr-stained cells, confirming the efflux pump inhibition by SMA (Fig. 1F(i) and (ii)). Consequently, the interference of the efflux machinery by SMA will lead to increased intracellular antibiotic concentrations and alleviation of drug resistance.

Therefore, the inhibitory effect of SMA on efflux pumps offers a promising mechanism to counteract drug resistance, as it enhances the intracellular concentration of antibiotics and combats the efflux-mediated resistance mechanism.

Accumulation of antibiotics inside bacteria

To further investigate the impact of SMA on antibiotic accumulation inside the bacterial cells, we examined the uptake of minocycline, a model antibiotic known to be resistant due to the activity of transmembrane efflux pumps. Minocycline exhibits fluorescence upon binding to the 30S subunit of bacterial ribosomes but is expelled by bacterial efflux pumps.[33] In the presence of the potentiator SMA, we performed a minocycline uptake assay in NDM-1-producing bacteria, specifically *K. pneumoniae* R3934. Remarkably, the addition of SMA resulted in an increase in fluorescence intensity, confirming the enhanced accumulation of minocycline inside the bacterial cells (Fig. 1G). This observation underscores the ability of SMA to elevate the intracellular concentration of antibiotics, reinforcing the potency of combination therapy involving SMA. The enhanced intracellular antibiotic concentration achieved through the use of SMA holds great promise for overcoming efflux-mediated resistance mechanisms and improving the efficacy of antibiotic treatments. This strategy represents a significant advancement in mitigating the challenges posed by antimicrobial resistance.

Bactericidal kinetics and visual turbidity assay

To demonstrate the bactericidal efficacy of the combination therapies, we conducted time-kill kinetics experiments using SMA in combination with three obsolete antibiotics (fusidic acid, chloramphenicol, or minocycline) against New Delhi metallo-β-lactamase-1 (NDM-1) producing Gram-negative pathogens. In addition to spread plating the treated bacterial cell suspensions onto solid agar media, we employed a visual turbidity test to further validate the effectiveness of the combination therapy (Fig. 2A and B).

The combination of SMA (16 μg mL^{-1}) and fusidic acid (4 μg mL^{-1}) completely eliminated NDM-1 producing *A. baumannii* A-

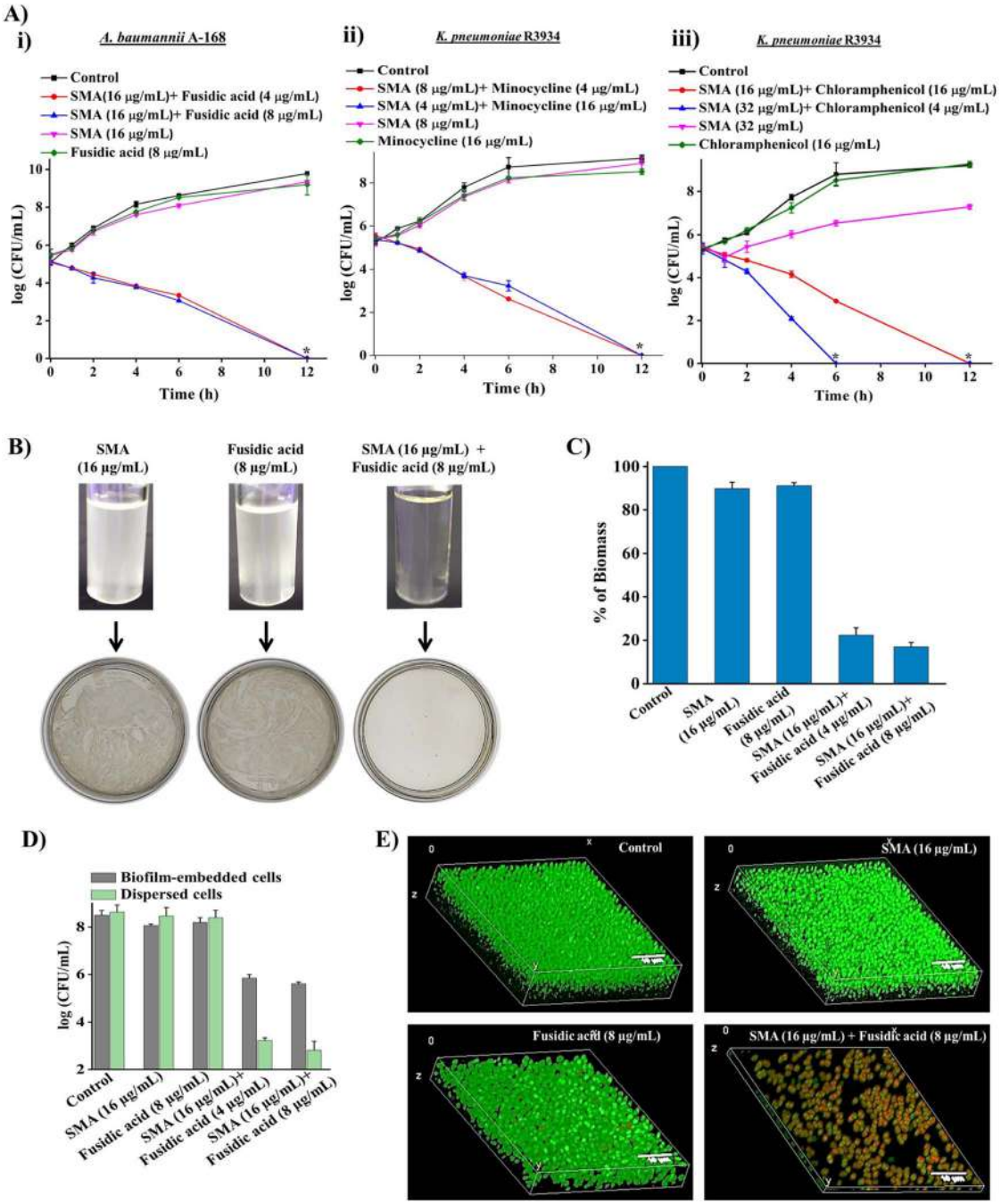

Fig. 2 Bactericidal activity of combination therapies, (A) time-kill kinetics of the combinations consisting of (i) SMA and fusidic acid against *A. baumannii* A168, (ii) SMA and minocycline against *K. pneumoniae* R3934, and (iii) SMA and chloramphenicol against *K. pneumoniae* R3934, the asterisk indicates complete killing and the detection limit of experiment was <50 CFU mL; (B) visual turbidity of the combination of SMA and fusidic acid against *A. baumannii* A168; biofilm disruption ability against the preformed biofilm of *A. baumannii* A168; (C) percentage of biomass after treatment through crystal violet staining; (D) viability of the biofilm-embedded bacteria and dispersed cells after treatment; (E) 3D reconstruction of z-stack images of the biofilm after treatment, by imaging by confocal laser scanning microscopy through co-staining with SYTO-9 (green fluorescence; stained both live and dead cells) and PI (red fluorescence; stained dead cells); merged images represented with thickness. Scale bar: 10 μm.

168 within 12 h, resulting in a 5.3 log reduction in bacterial count. Notably, the growth media containing the SMA and fusidic acid cocktail showed no visual turbidity, and there were no bacterial colonies on the solid agar. In contrast, bacterial suspensions treated with SMA (16 μg mL^{-1}) or fusidic acid (8 μg mL^{-1}) alone displayed turbidity in the solution and abundant bacterial growth on the agar plate (Fig. 2A(i) and 2B).

Similarly, the combination of SMA (8 μg mL^{-1}) and minocycline (4 μg mL^{-1}) completely eradicated NDM-1 producing *K. pneumoniae* R3934 within 12 h, resulting in a 5.2 log reduction

in bacterial burden. In contrast, when SMA (8 μg mL^{-1}) or minocycline (4 μg mL^{-1}) was used as individual treatments, the bacterial count increased by ~8 log, similar to the untreated control. The visual turbidity experiment and spread plating of the treated bacterial suspension also confirmed the potent efficacy of the SMA-minocycline combination against NDM-1 producing *K. pneumoniae* strains (Fig. 2A(ii) and S8A†).

Furthermore, the combinations of SMA (32 μg mL^{-1}) with chloramphenicol (4 μg mL^{-1}) and SMA (16 μg mL^{-1}) with chloramphenicol (16 μg mL^{-1}) completely eliminated the tested NDM-1 producing bacteria *K. pneumoniae* R3934 within 6 h and 12 h, respectively, resulting in a 5.4 log reduction in bacterial burden. In contrast, treatment with chloramphenicol alone at a concentration of 16 μg mL^{-1} increased bacterial viability to 9 log, similar to the untreated control, within 12 h (Fig. 2A(iii) and S8B†).

In summary, the SMA molecule effectively repurposed various classes of antibiotics against critical NDM-1 producing Gram-negative pathogens, leading to complete eradication of bacterial burden in the solution phase. Based on the promising results, we selected the combination therapy of SMA and fusidic acid for further studies, as it demonstrated the potential to repurpose fusidic acid, which is typically prescribed for treating Gram-positive bacterial infections, against multi-drug resistant (MDR) Gram-negative superbugs.

Biofilm disruption ability against NDM-1 producing bacteria

Biofilm-mediated infections pose a serious threat to global health as they are resistant to conventional antibiotics. Biofilms are composed of millions of bacterial cells surrounded by a self-generated extracellular polymeric matrix (EPM).[7] Unfortunately, the rigid EPS matrix renders most conventional antibiotics ineffective against biofilms. This situation is further exacerbated when dealing with biofilms formed by multidrug-resistant Gram-negative pathogens. Therefore, there is a critical need to develop potent anti-biofilm agents.

To address this challenge, we investigated the biofilm disruption efficacy of the leading combination therapy of SMA and fusidic acid against NDM-1 producing *A. baumannii* A168 biofilms. Crystal violet staining confirmed that the combination therapy of SMA (16 μg mL^{-1}) and fusidic acid (4 μg mL^{-1}) effectively disrupted the preformed biofilm of NDM-1 producing *A. baumannii*. In contrast, treatment with fusidic acid alone did not help penetrate the preformed biofilm (Fig. 2C). Additionally, we quantified the viability of bacteria embedded within the biofilm. Interestingly, SMA and fusidic acid alone did not significantly reduce the cell count in the preformed biofilm. However, the combination of SMA (16 μg mL^{-1}) and fusidic acid (4 μg mL^{-1}), as well as SMA (16 μg mL^{-1}) and fusidic acid (8 μg mL^{-1}), resulted in 2.5 log (>99% killing) and 3 log (~99.9% killing) reduction in viable bacterial count within the NDM-1 producing *A. baumannii* biofilm-embedded bacteria, respectively (Fig. 2D). Moreover, this combination therapy exhibited potent bactericidal efficacy against biofilm-dispersed cells, including metabolically dormant cells. The combination of SMA (16 μg mL^{-1}) and fusidic acid (4 μg mL^{-1}) reduced the bacterial burden by 5.6 log in the dispersed cells of the *A. baumannii* A-168 biofilm (Fig. 2D).

Furthermore, we visualized the biofilm disruption ability and eradication of biofilm-embedded bacteria using confocal laser scanning microscopy (CLSM) with instantaneous staining using SYTO-9 (green fluorescence) and propidium iodide (PI: red fluorescence) dyes. SYTO-9 stains both live and dead bacterial cells, while PI specifically stains only dead cells. In the control biofilm, all cells were stained green, confirming the presence of live cells, and the biofilm thickness measured 8.5 μm. In the case of individual treatment with SMA or fusidic acid, all cells were green fluorescence-stained, indicating the presence of live cells, and the biofilm thickness measured 7.2 μm and 8.1 μm, respectively. However, treatment with the combination therapy of SMA and fusidic acid remarkably reduced the thickness of the preformed biofilm to 1.2 μm (Fig. 2E). In contrast, the combination-treated biofilm-embedded bacteria exhibited staining with both green and red fluorescence, confirming the killing of viable bacteria within the biofilm. Overall, SMA not only facilitated the disruption of the preformed biofilm but also repurposed fusidic acid to eliminate biofilm-embedded NDM-1 producing *A. baumannii* bacteria.

Antibacterial efficacy of combination therapy against multispecies bacterial co-culture

Multispecies bacterial co-infections are commonly observed under conditions such as lung infections, cystic fibrosis, and diabetic wound infections.[34] When treating these critical multispecies bacterial co-infections, doctors often prescribe combination therapies using different types of antibiotics. However, conventional antibiotics are increasingly becoming ineffective in tackling these co-infections, leading to the emergence of drug resistance.[35] Therefore, novel strategies are needed to address this challenge. In this study, we evaluated the efficacy of the leading combination therapy against a multispecies bacterial co-culture comprising Gram-positive and Gram-negative bacteria. SMA demonstrated potent anti-staphylococcal activity against vancomycin-susceptible and vancomycin-resistant strains (Table S1†). Furthermore, SMA repurposed fusidic acid to target MDR Gram-negative bacteria. Consequently, we investigated the effectiveness of the combination of SMA and fusidic acid against a multispecies co-culture of MRSA ATCC33591 and NDM-1 producing *A. baumannii* A168 bacteria. The anti-MRSA agent SMA (16 μg mL^{-1}), both alone and in combination with fusidic acid (8 μg mL^{-1}), completely eliminated the MRSA bacterial burden in the co-culture, resulting in a 5.2 log reduction within 12h. Fusidic acid exhibited a static effect against the MRSA bacterial burden in the co-culture with *A. baumannii*. The well-known antibiotic vancomycin (16 μg mL^{-1}) reduced the viability of MRSA bacteria by 0.7 log within 12 h. Surprisingly, both SMA and fusidic acid alone increased the viability of *A. baumannii* A168 to 8.2 log within 12 h in the co-culture with MRSA. Similarly, the viability of *A. baumannii* in the co-culture treated with colistin (8 μg mL^{-1}) also increased to 8 log within 12 h. Remarkably, the combination of SMA and fusidic acid achieved a ~2.2 log reduction (>99% killing) in the

A. baumannii bacterial burden within the co-culture with MRSA (Fig. 3A(i)). The visual turbidity test also confirmed the potent efficacy of the leading combination (Fig. 3A(ii)). In conclusion, the combination therapy of SMA and fusidic acid demonstrated effectiveness in eliminating the multispecies bacterial co-culture.

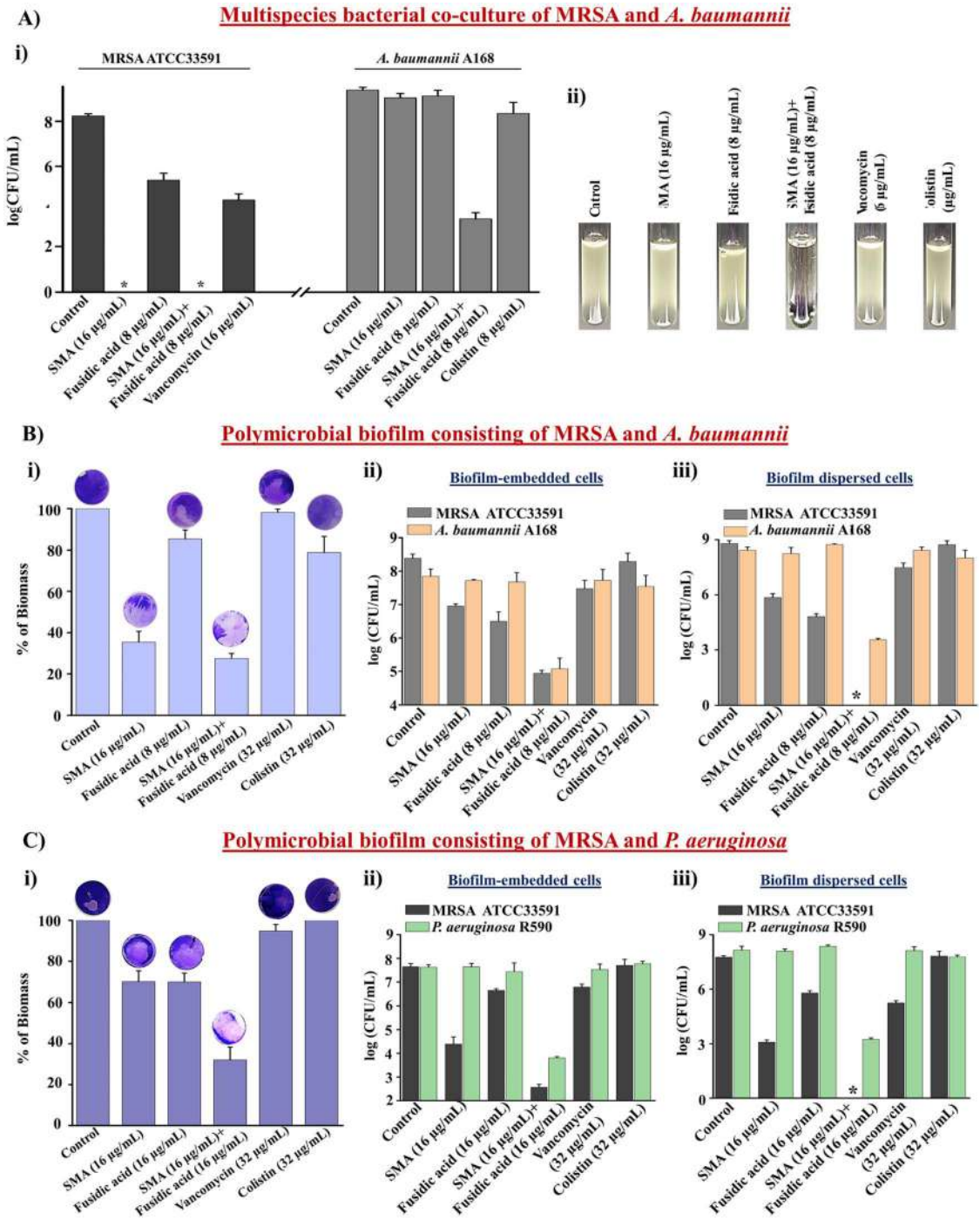

Fig. 3 (A) Bactericidal efficacy of the combination of SMA + fusidic acid against multispecies bacterial co-culture of MRSA ATCC33591 and *A. baumannii* A168; (i) viable bacterial count in multispecies bacterial co-culture, and (ii) visual turbidity test of multispecies bacterial co-culture, asterisks indicate complete killing; (B) anti-biofilm efficacy of the combination of SMA + fusidic acid against the polymicrobial biofilm consisting of both MRSA ATCC33591 and *A. baumannii* A168, (i) percentage of biomass after treatment, (ii) no. of viable biofilm-embedded bacteria, and (iii) no. of viable bacteria in biofilm dispersed cells; (C) anti-biofilm efficacy of the combination of SMA + fusidic acid against the polymicrobial biofilm consisting of both MRSA ATCC33591 and *P. aeruginosa* R590, (i) percentage of biomass after treatment, (ii) no. of viable biofilm-embedded bacteria, and (iii) no. of viable bacteria in biofilm dispersed cells, asterisks indicate complete killing. The detection limit of the experiment was <50 CFU mL^{-1}.

Anti-biofilm efficacy of combination therapy against the multispecies bacterial biofilm

The significant reduction observed in the multispecies bacterial co-culture experiment prompted us to evaluate the efficacy of the lead cocktail (fusidic acid + SMA) against more complex multispecies bacterial biofilms. A preformed biofilm of MRSA ATCC33591 and NDM-1 producing *A. baumannii* A-168 was grown on coverslips and subsequently treated with the combination therapy. Crystal violet staining confirmed that SMA and fusidic acid individually reduced the biofilm biomass by 70% and 17% respectively. The control antibiotics, vancomycin and colistin, reduced the biofilm biomass by 7% and 22%, respectively. In contrast, the combination of SMA (16 μg mL^{-1}) and fusidic acid (8 μg mL^{-1}) achieved a remarkable 75% reduction in the biomass of the multispecies biofilm (Fig. 3B(i)). Moreover, the combination treatment of SMA (16 μg mL^{-1}) and fusidic acid (8 μg mL^{-1}) eliminated 3.2 log MRSA bacterial burden within the multispecies biofilm. Individually, the anti-MRSA agents SMA and fusidic acid achieved reductions of 1.4 log and 1.7 log, respectively, in the MRSA bacterial burden within the biofilm. The blockbuster antibiotic, vancomycin (32 μg mL^{-1}), only achieved a 1 log reduction in the MRSA bacterial burden within the preformed biofilm. Additionally, the combination therapy effectively reduced the *A. baumannii* bacterial burden by 3.2 log within the multispecies biofilm. In contrast, SMA and fusidic acid individually were ineffective against *A. baumannii* bacteria embedded in the multispecies biofilms. Similarly, colistin (32 μg mL^{-1}) failed to eliminate the biofilm-embedded *A. baumannii* bacteria (Fig. 3B(ii)). Furthermore, this combination therapy demonstrated potent bactericidal efficacy against the dispersed cells within the multispecies biofilm, targeting various phases of bacterial cells. The combination of SMA (16 μg mL^{-1}) and fusidic acid (8 μg mL^{-1}) achieved complete elimination of the bacterial burden (8.5 log reduction) of MRSA and reduced the *A. baumannii* A168 bacterial burden by 4.6 log in the dispersed cells of the mixed-species biofilm (Fig. 3B(iii)). Similarly, the combination of SMA and fusidic acid effectively disrupted the preformed multispecies biofilm of MRSA and *P. aeruginosa* R590, resulting in a 70% reduction in biomass (Fig. 3C(i)). Furthermore, it successfully killed both MRSA and *P. aeruginosa* bacteria within the biofilm, achieving a 5.1 log reduction for MRSA and a 3.8 log reduction for *P. aeruginosa* (Fig. 3C(ii)). Additionally, the combination therapy demonstrated efficacy against the dispersed cells, resulting in a 7.7 log reduction for MRSA and a 5.9 log reduction for *P. aeruginosa* (Fig. 3C(iii)). In contrast, vancomycin (32 μg mL^{-1}) and colistin (32 μg mL^{-1}) treatments were ineffective against this multispecies bacterial biofilm comprising MRSA and *P. aeruginosa*. In conclusion the cocktail therapy of SMA and fusidic acid has the potential to effectively combat biofilm-mediated multispecies bacterial infections.

In vitro cytotoxicity of lead combinations

Furthermore, we investigated the cytotoxicity of the leading combinations against the human embryonic kidney cell line (HEK- 293T) using the LIVE/DEAD assay, which involved staining with calcein-AM (green fluorescence) and PI (red fluorescence). The combination of SMA (16 μg mL^{-1}) and fusidic acid (32 μg mL^{-1}) treated cells exhibited green staining only, indicating that the cells were alive, similar to the control group. In contrast, cells treated with Triton-X were solely stained with PI, confirming cell death. Therefore, the lead combination therapy demonstrated remarkable biocompatibility with mammalian cells (Fig. 4A). It is worth noting that the cytotoxicity of SMA alone has been previously reported.[21]

In vivo systemic toxicity of SMA

To assess the therapeutic applicability, we investigated the *in vivo* systemic toxicity of SMA by administering different dosages *via* intra-peritoneal and subcutaneous injections, following the guidelines provided by OECD 425. In the case of intra-peritoneal administration, SMA exhibited a considerable LD_{50} (lethal dose for 50% mortality) of 130 mg kg^{-1}. However, when administered subcutaneously at a dosage of 175 mg kg^{-1}, all mice survived without any adverse effects. Therefore, the LD_{50} of SMA for subcutaneous administration was determined to be >175 mg kg^{-1}. These results indicate that SMA exhibits biocompatibility for both systemic and topical applications in combination therapy (Fig. 4B).

Resistance frequency

The emergence of drug resistance poses a significant obstacle to the development and approval of new antimicrobials. In order to address this concern, we determined the frequency of resistance development against the lead combination therapy of SMA and fusidic acid, using NDM-1 producing *A. baumannii* A168 bacteria. 100 μL of bacterial suspension of various concentrations (ranging from 10^9 CFU to 10^5 CFU) were spread-plated on nutrient agar plates containing either the combination of SMA and fusidic acid, fusidic acid alone, or colistin and then incubated for 24 h. At a bacterial concentration of 3×10^6 CFU on the plate containing 512 μg mL^{-1} (8 × MIC) of fusidic acid alone, we observed the presence of 40 resistant mutants, resulting in a frequency of resistance of *A. baumannii* against fusidic acid alone at 1.3×10^{-5}. On the other hand, when the combination therapy of SMA (16 μg mL^{-1}) and fusidic acid (4 μg mL^{-1}) was tested against bacterial suspensions of 3×10^8 CFU, we observed 51 resistant mutants, yielding a frequency of resistance against the combination therapy at 1.7×10^{-7}. Similarly, the presence of 55 resistant *A. baumannii* mutants indicated a resistance frequency against colistin at 8 μg mL^{-1} (8 × MIC) of 1.8×10^{-8} (Fig. 4C). These results collectively indicate that NDM-1 producing *A. baumannii* bacteria are less prone to developing spontaneous resistance against the combination of SMA and fusidic acid compared to fusidic acid alone, even at very high concentrations. This may be attributed to the enhanced intracellular concentration of the antibiotics in the presence of SMA, which potentially contributes to the reduced resistance development.

In vivo antibacterial efficacy of combination therapy

The *in vivo* antibacterial activity of the lead combination therapy comprising SMA and fusidic acid was evaluated using a murine

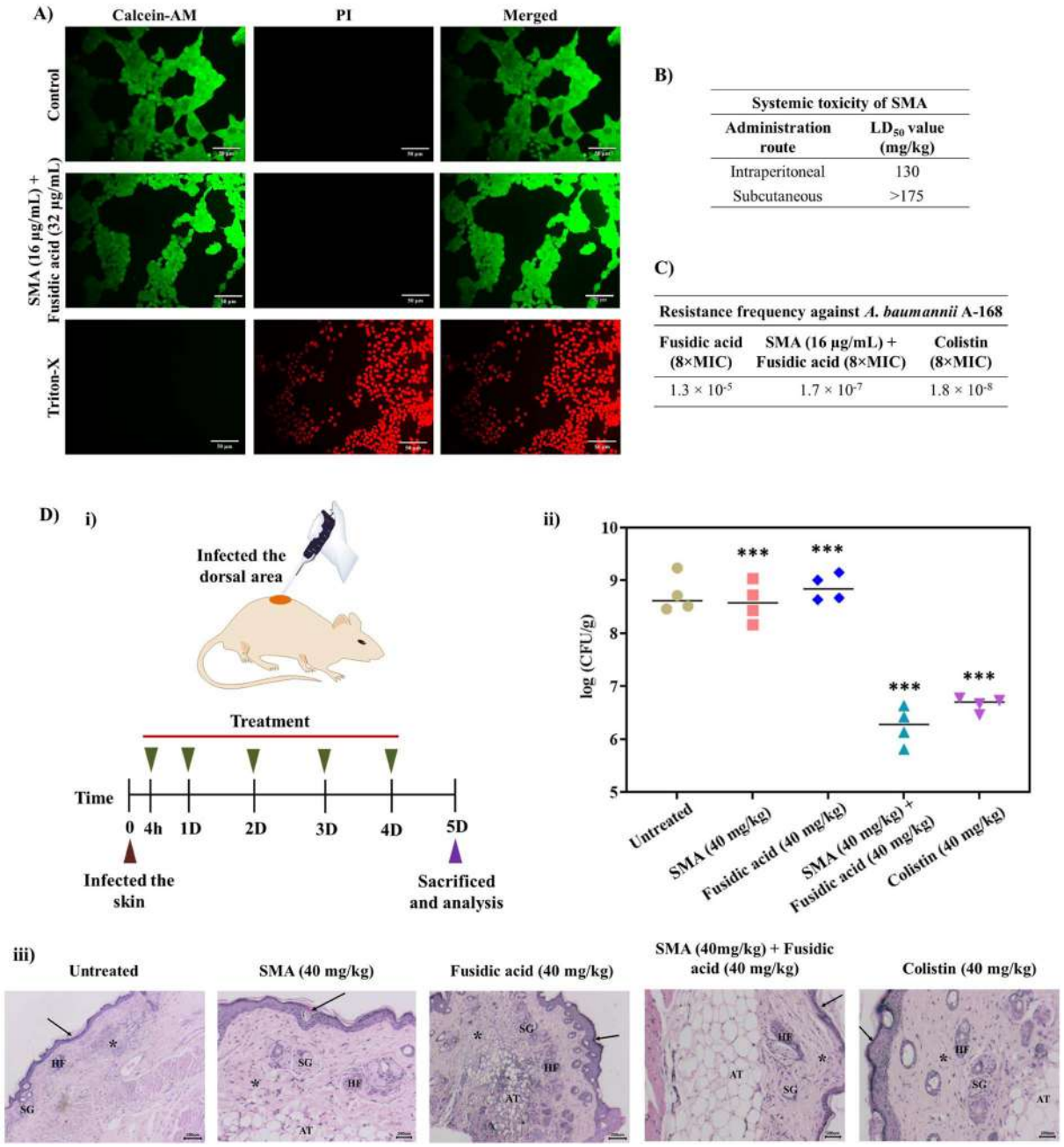

Fig. 4 (A) Biocompatibility of the leading combinations against the mouse HEK-293T cell line by performing the LIVE/DEAD assay through staining with calcein-AM (green fluorescence; stained live cells) and PI (red fluorescence; stained dead cells); merged channel images are represented; scale bar: 50 μm; (B) *in vivo* systemic toxicity of SMA through different routes of administration in the mouse model. (C) Frequency of resistance growth by NDM-1 producing bacteria *A. baumannii* A168 against the leading combinations; (D) *in vivo* antibacterial efficacy of the combination consisting of SMA and fusidic acid; (i) the experimental design of the mouse skin infection model with *A. baumannii* A168 bacteria, (ii) number of viable bacteria in the skin tissue sample upon treatment, and (iii) mice infected skin tissue histology. Scale bar: 200 μm. In untreated and SMA and fusidic acid treatment cases, severe to moderate inflammatory cell infiltration is shown (asterisks), whereas the combination treatment tissue sample and colistin tissue sample revealed minimum inflammatory cell infiltration (asterisks). Arrows indicate the keratin layer; sebaceous glands (SG); hair follicles (HF); adipose tissue (AT).

skin infection model. Briefly, the skin of the mice was infected with $\sim 10^6$ CFU mL^{-1} (per mouse) of NDM-1 producing *A. baumannii* A168. After 4 h of infection, the infected skin was treated with different antimicrobial agents for up to 4 days, with a single dosage administered each day. On day five, all animals were sacrificed and skin tissues were collected and homogenised in saline to determine the bacterial viability in the infected tissues (Fig. 4D(i)). In the untreated group (washed with saline daily), the bacterial burden was increased to $\sim 8.7 \times 10^8$ CFU g^{-1}. Treatment with only SMA (40 mg kg^{-1}) resulted in

a modest reduction of 0.2 log compared to the untreated case. However, the individual treatment of fusidic acid failed to decrease the bacterial burden in the infected skin, with a count of viable bacteria at $\sim 8.8 \times 10^8$ CFU g^{-1}, similar to the untreated case. Interestingly, the combination therapy of SMA and fusidic acid exhibited potent *in vivo* antibacterial efficacy. In mice treated with the combination of SMA (40 mg kg^{-1}) and fusidic acid (40 mg kg^{-1}), the bacterial viability of NDM-1 producing bacteria *A. baumannii* was reduced by $\sim$2.5 log compared to the untreated case. Colistin also demonstrated superior activity, reducing the bacterial viability by $\sim$2.1 log in this murine skin infection model (Fig. 4D(ii)). Furthermore, histopathological studies were conducted on the tissue samples from all groups. In the untreated group and in mice treated with SMA or fusidic acid individually, the corresponding tissue samples exhibited severe to moderate infiltration of inflammatory cells and damaged cells. In contrast, the combination-treated tissues showed a normal appearance of the keratin layer, adipose tissue, and sebaceous glands, with minimal infiltration of inflammatory cells (Fig. 4D(iii)). Collectively, these results indicate that the combination therapy of SMA and fusidic acid demonstrates potent efficacy in combating NDM-1 producing bacterial-induced topical infections, surpassing the effects of individual treatments. These findings hold great promise for the development of an innovative antibacterial strategy to address infections caused by multi-drug resistant Gram-negative pathogens.

Conclusions

Combining antibiotics with membrane-targeting molecules represents a frontline approach in the battle against antimicrobial resistance (AMR), as targeting the bacterial membrane offers a smart alternative. In this study, we have demonstrated the remarkable potentiation efficacy of a small amphiphilic molecule called SMA against various classes of obsolete antibiotics, including rifampicin, minocycline, fusidic acid, and chloramphenicol, against a range of multi-drug resistant Gram-negative bacteria. The combination of SMA and antibiotics exhibited potent bactericidal activity against NDM-1 producing planktonic Gram-negative bacterial cells. Moreover, it effectively eradicated bacteria embedded within the preformed biofilms of NDM-1 producing *A. baumannii*. SMA was found to inhibit bacterial efflux pumps, leading to increased accumulation of antibiotics inside bacterial cells. Given the escalating bacterial resistance, treating multispecies bacterial infections has become a critical challenge in the healthcare system. However, the combination of SMA (an anti-MRSA agent) and fusidic acid demonstrated potent bactericidal activity against both MRSA and NDM-1 producing *A. baumannii* in multispecies bacterial co-cultures and their preformed biofilms. Importantly, the lead combination exhibited biocompatibility with mammalian RAW cell lines. *In vivo* studies using a mouse model demonstrated the high LD_{50} value of SMA, indicating its safety for systemic use. Furthermore, the combination therapy exhibited excellent antibacterial efficacy in a mouse skin infection model. Notably, *A. baumannii* exhibited slow development of resistance against the combination therapy. Overall, this combination therapy holds enormous potential as a novel strategy to combat antimicrobial resistance in Gram-negative superbugs.

Ethical statement

The Institutional Bio-Safety Committee of the Jawaharlal Nehru Centre for Advanced Scientific Research approved the antibacterial studies, which also included hemolytic activities (JNC/IBSC/2020/JH-12). The *in vivo* experiments were conducted in accordance with the guidelines approved by the Jawaharlal Nehru Centre for Advanced Scientific Research's Institutional Animal Ethics Committee (IAEC) (201/Go/ReBi/S/2000/CPCSEA).

Data availability

The authors declare that all data supporting the findings of this study are available within the article and ESI,† and raw data files are available from the corresponding authors upon request.

Author contributions

The work and the experiments were designed by R. D. and J. H. Cell toxicity assay was performed by R. M. All other studies were conducted by R. D., S. M., and R. M. All the data were analyzed by R. D., R. M., and J. H. The manuscript was written by R. D., S. M., and J. H. All the authors approved the final version of the manuscript.

Conflicts of interest

There are no conflicts to declare.

Acknowledgements

R. D. acknowledges CSIR for a Senior Research Fellowship (SRF). S. M. thanks JNCASR for funding. The authors acknowledge Rohana Veterinary Diagnostic Laboratory (Bangalore, Karnataka, India) and R. V. Metropolis Clinical Laboratory (Bangalore, Karnataka, India) for assistance in *in vivo* studies. R. D. thanks Geetika Dhanda for various helpful scientific discussions.

References

1 GBD 2019 Antimicrobial Resistance Collaborators, *Lancet*, 2023, **400**, 2221.
2 C. Ghosh, P. Sarkar, R. Issa and J. Haldar, Alternatives to conventional antibiotics in the era of antimicrobial resistance, *Trends Microbiol.*, 2019, **27**, 323.
3 E. Tacconelli, E. Carrara, A. Savoldi, S. Harbarth, M. Mendelson, D. L. Monnet, C. Pulcini, G. Kahlmeter, J. Kluytmans and Y. Carmeli, WHO Pathogens Priority List Working Group, *Lancet Infect. Dis.*, 2018, **18**, 318.
4 R. A. Garibaldi, *J. Hosp. Infect.*, 1999, **43**, S9.

5 C. D. Russell, C. J. Fairfield, T. M. Drake, L. Turtle, R. A. Seaton, D. G. Wootton, L. Sigfrid, E. M. Harrison, A. B. Docherty, T. I. De Silva, C. Egan, R. Pius, H. E. Hardwick, L. Merson, M. Girvan, J. Dunning, J. S. Nguyen-Van-Tam, J. S. Openshaw, J. K. Baillie, M. G. Semple and A. Ho, *Lancet Microbe*, 2021, **2**, e354.
6 N. Shafran, I. Shafran, H. Ben-Zvi, S. Sofer, L. Sheena, I. Krause, A. Shlomai, E. Goldberg and E. H. Sklan, *Sci. Rep.*, 2021, **11**, 12703.
7 C. J. L. Murray, K. S. Ikuta, F. Sharara, L. Swetschinski, A. G. Robles, A. Gray, C. Han, C. Bisignano, P. Rao, E. Wool, S. C. Johnson, A. J. Browne, M. G. Chipeta, F. Fell and S. Hackett, *Lancet*, 2022, **399**, 629.
8 C. R. MacNair, J. M. Stokes, L. A. Carfrae, A. A. Fiebig-Comyn, B. K. Coombes, M. R. Mulvey and E. D. Brown, *Nat. Commun.*, 2018, **9**, 458.
9 M. Vaara, *Molecules*, 2019, **24**, 249.
10 E. van Groesen, C. J. Slingerland, P. Innocenti, M. Mihajlovic, R. Masereeuw and N. I. Martin, *ACS Infect. Dis.*, 2021, **7**, 2746.
11 P. Brown, E. Abbott, O. Abdulle, S. Boakes, S. Coleman, N. Divall, E. Duperchy, S. Moss, D. Rivers, M. Simonovic, J. Singh, S. Stanway, A. Wilson and M. J. Dawson, *ACS Infect. Dis.*, 2019, **5**, 1645.
12 M. Song, Y. Liu, X. Huang, S. Ding, Y. Wang, J. Shen and K. Zhu, *Nat. Microbiol.*, 2020, **5**, 1040.
13 J. M. Stokes, C. R. MacNair, B. Ilyas, S. French, J.-P. Côté, C. Bouwman, M. A. Farha, A. O. Sieron, C. Whitfield, B. K. Coombes and E. D. Brown, *Nat. Microbiol.*, 2017, **2**, 17028.
14 A. Cannatelli, S. Principato, O. L. Colavecchio, L. Pallecchi and G. M. Rossolini, *Front. Microbiol.*, 2018, **9**, 1808.
15 M. M. Konai and J. Haldar, *ACS Infect. Dis.*, 2020, **6**, 91.
16 G. Blankson, A. K. Parhi, M. Kaul, D. S. Pilch and E. J. LaVoie, *Eur. J. Med. Chem.*, 2019, **178**, 30.
17 G. D. Wright, *Trends Microbiol.*, 2016, **24**, 862.
18 H. Douafer, V. Andrieu, O. Phanstiel and J. M. Brunel, *J. Med. Chem.*, 2019, **62**, 8665.
19 M. Chang, K. V. Mahasenan, J. A. Hermoso and S. Mobashery, *Acc. Chem. Res.*, 2021, **54**, 917.
20 R. Dey, S. Mukherjee, S. Barman and J. Haldar, *Macromol. Biosci.*, 2021, **21**, 2100182.
21 R. Dey, K. De, R. Mukherjee, S. Ghosh and J. Haldar, *MedChemComm*, 2019, **10**, 1907.
22 P. J. F. Henderson, C. Maher, L. D. H. Elbourne, B. A. Eijkelkamp, I. T. Paulsen and K. A. Hassan, *Chem. Rev.*, 2021, **121**, 5417.
23 M. A. Webber and L. J. V. Piddock, *J. Antimicrob. Chemother.*, 2003, **51**, 9.
24 D. Ma, D. N. Cook, J. E. Hearst and H. Nikaido, *Trends Microbiol.*, 1994, **2**, 489.
25 A. Cauilan and C. Ruiz, *Pathogens*, 2022, **11**, 1409.
26 D. Corbett, A. Wise, T. Langley, K. Skinner, E. Trimby, S. Birchall, A. Dorali, S. Sandiford, J. Williams, P. Warn, M. Vaara and T. Lister, *Antimicrob. Agents Chemother.*, 2017, **61**, e00200.
27 M. Besouw, R. Masereeuw, L. van den Heuvel and E. Levtchenko, *Drug Discovery Today*, 2013, **18**, 785.
28 G. Dhanda, Y. Acharya and J. Haldar, *ACS Omega*, 2023, **8**, 10757.
29 K. Klobucar and E. D. Brown, *Curr. Opin. Chem. Biol.*, 2022, **66**, 102099.
30 B. J. Berry, A. J. Trewin, A. M. Amitrano, M. Kim and A. P. Wojtovich, *J. Mol. Biol.*, 2018, **430**, 3873.
31 D. G. J. Larsson and C. F. Flach, *Nat. Rev. Microbiol.*, 2022, **20**, 257.
32 S. J. Howard, M. Catchpole, J. Watson and S. C. Davies, *Lancet Infect. Dis.*, 2013, **13**, 1001.
33 G. Dhanda, R. Mukherjee, D. Basak and J. Haldar, *ACS Infect. Dis.*, 2022, **8**, 1086.
34 J. R. Gaston, A. O. Johnson, K. L. Bair, A. N. White and C. E. Armbruster, *Infect. Immun.*, 2021, **89**, e00652.
35 B. M. Peters, M. A. Jabra-Rizk, G. A. O'May, J. W. Costerton and M. E. Shirtliff, *Clin. Microbiol. Rev.*, 2012, **25**, 193.